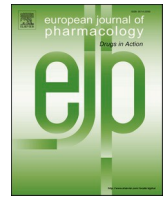Since January 2020 Elsevier has created a COVID-19 resource centre with free information in English and Mandarin on the novel coronavirus COVID-19. The COVID-19 resource centre is hosted on Elsevier Connect, the company's public news and information website.

Assessment of proarrhythmogenic risk for chloroquine and hydroxychloroquine using the CiPA concept

Urs Thomet [a], Bogdan Amuzescu [b,*], Thomas Knott [c], Stefan A. Mann [d], Kanigula Mubagwa [e,f], Beatrice Mihaela Radu [b]

[a] *Anaxon A.G., Brünnenstrasse 90, 3018, Bern, Switzerland*
[b] *Dept. Anatomy, Animal Physiology & Biophysics, Faculty of Biology, University of Bucharest, Splaiul Independentei 91-95, 050095, Bucharest, Romania*
[c] *CytoBioScience Inc., 3463 Magic Drive, San Antonio, TX, 78229, USA*
[d] *Cytocentrics Bioscience GmbH, Nattermannallee 1, 50829, Cologne, Germany*
[e] *Dept. Cardiovascular Sciences, Faculty of Medicine, K U Leuven, B-3000, Leuven, Belgium*
[f] *Dept. Basic Sciences, Faculty of Medicine, Université Catholique de Bukavu, Bukavu, DR Congo*

ABSTRACT

Chloroquine and hydroxychloroquine have been proposed recently as therapy for SARS-CoV-2-infected patients, but during 3 months of extensive use concerns were raised related to their clinical effectiveness and arrhythmogenic risk. Therefore, we estimated for these compounds several proarrhythmogenic risk predictors according to the Comprehensive *in vitro* Proarrhythmia Assay (CiPA) paradigm. Experiments were performed with either CytoPatch™2 automated or manual patch-clamp setups on HEK293T cells stably or transiently transfected with hERG1, hNav1.5, hKir2.1, hKv7.1+hMinK, and on Pluricyte® cardiomyocytes (Ncardia), using physiological solutions. Dose-response plots of hERG1 inhibition fitted with Hill functions yielded IC50 values in the low micromolar range for both compounds. We found hyperpolarizing shifts of tens of mV, larger for chloroquine, in the voltage-dependent activation but not inactivation, as well as a voltage-dependent block of hERG current, larger at positive potentials. We also found inhibitory effects on peak and late I_{Na} and on I_{K1}, with IC50 of tens of μM and larger for chloroquine. The two compounds, tested on Pluricyte® cardiomyocytes using the β-escin-perforated method, inhibited I_{Kr}, I_{CaL}, $I_{Na\ peak}$, but had no effect on I_f. In current-clamp they caused action potential prolongation. Our data and those from literature for I_{to} were used to compute proarrhythmogenic risk predictors B_{net} (Mistry HB, 2018) and Q_{net} (Dutta S et al., 2017), with hERG1 blocking/unblocking rates estimated from time constants of fractional block. Although the two antimalarials are successfully used in autoimmune diseases, and chloroquine may be effective in atrial fibrillation, assays place these drugs in the intermediate proarrhythmogenic risk group.

1. Introduction

Chloroquine and hydroxychloroquine are two classical quinoline antimalarials derived from quinine, extracted by indigenous inhabitants of South America from the bark of *Cinchona officinalis* and used for centuries as a remedy for chills and common cold. Chloroquine was synthesized in 1934 by Johann (Hans) Andersag at Bayer A.G. by replacing the acridine with a quinoline ring in quinacrine (Atabrine) and was used under the name Resochin; in 1945 it was rediscovered by E.K. Marshall and received its current name (Krafts et al., 2012), remaining for decades a first-line antimalarial therapy. The mechanisms of action

of quinoline antimalarials in autoimmune diseases are complex (Chew et al., 2020; Haładyj et al., 2018; Wallace, 1989).

The antiviral activity of chloroquine and hydroxychloroquine is deemed to result from accumulation of the protonated charged form in the acidic environment of endosomes, lysosomes and Golgi vesicles, leading to increased internal endosomal pH, thus preventing their use by viral particles as entry gateways (Ducharme and Farinotti, 1996). Chloroquine has been tested *in vitro* or *in vivo* and found effective against Zika virus (Li et al., 2017a), influenza A H5N1 (avian flu) (Yan et al., 2013), Dengue virus type 2 (Farias et al., 2015), and some coronaviruses including OC43 (Keyaerts et al., 2009) and SARS-CoV-1 (Keyaerts et al.,

2004). Other studies suggested supplementary protective mechanisms of chloroquine against SARS-CoV-1, including terminal glycosylation of ACE2 resulting in decreased affinity for the viral spike protein (Vincent et al., 2005).

Preliminary *in vitro* studies of effectiveness against SARS-CoV-2 found EC50 values of 1.13–5.47 μM for chloroquine (Wang et al., 2020; Yao et al., 2020) or, and 0.72–1.38 μM for hydroxychloroquine (Yao et al., 2020; Yuan et al., 2020). These values are higher than maximal free plasma therapeutic concentrations (C_{max}) estimated at 0.41 μM for chloroquine (Borsini et al., 2012) and 0.495 μM (215 ng/ml) for hydroxychloroquine (Yao et al., 2020) taken in usual doses. Although initial small-scale clinical trials with chloroquine/hydroxychloroquine on coronavirus-infected patients reported positive results, subsequent randomized unbiased trials were negative (Gasmi et al., 2021; Hernandez et al., 2020; Horby et al., 2020; Kashour et al., 2021). Moreover, severe cardiac arrhythmias associated with QT prolongation were reported by many studies (Borba et al., 2020; Chorin et al., 2020; Gérard et al., 2020; Mercuro et al., 2020; Roden et al., 2020; Tleyjeh et al., 2020), including a retracted Lancet paper (Mehra et al., 2020; Piller, 2021). As a consequence, on June 15, 2020, the FDA revoked the EUA for hydroxychloroquine and chloroquine in clinical trials on coronavirus-infected patients (US Food and Drug Administration, 2020).

Given the arrhythmogenic effects of 4-aminoquinoline antimalarials (Mubagwa, 2020; Vicente et al., 2019), and the fact that SARS-CoV-2-infected patients often present myocardial injury by multiple mechanisms (Topol, 2020) and are highly susceptible to arrhythmias, the aim of our study was to perform an in-depth *in vitro* exploration of pharmacological effects of chloroquine and hydroxychloroquine on multiple human cardiac ion channels and to compute several proarrhythmogenic risk predictors following the principles and methods emerged from the CiPA initiative, a new paradigm for cardiac safety pharmacology (Fermini et al., 2016; Sager et al., 2014).

2. Materials and methods

2.1. Electrophysiology experiments on human ion channels expressed in heterologous cell lines

We used for experiments HEK293T cell lines stably or transiently expressing human cardiac ion channel subunits genes: stably expressed hERG1, inducible hNav1.5, inducible hKv7.1+hMinK, hKir2.1 included in a plasmid (pCWXPGR-pTF-Kir2.1, a gift from Patrick Salmon: Addgene plasmid #114284; http://n2t.net/addgene:114284; RRID:Addgene_114284). Transient transfection was done with LipoD293™ reagent (SignaGen® Laboratories) following manufacturer's instructions. Cell lines were seeded in multi-well plates and cultured in standard conditions (5% CO_2, 37°C) in humidified incubators. For passages or preparation of cell suspensions for automated patch-clamp experiments cells were detached by either 3-min treatment with trypsin-EDTA or 7-min treatment with Accutase® (A6964, Sigma-Aldrich) at 37°C. The cells were briefly centrifuged, resuspended in extracellular solution at high density for automated patch-clamp experiments or placed on 35-mm diameter Petri dishes in extracellular solution, and kept at 37°C for at least 30 min to adhere for manual patch-clamp experiments. For hNav1.5 and hKv7.1 experiments, cells were replated at low density on 35-mm diameter Petri dishes, and only isolated cells were approached by patch-clamp to avoid electrically coupled clusters of cells (Pritchett et al., 1988) where voltage cannot be rigorously clamped for the entire group of cells (Verdoorn et al., 1990).

Most electrophysiology experiments were performed at room temperature (RT: 22–25°C) with either automated or manual patch-clamp setups. For automated patch-clamp we used CytoPatch™2 Cytocentering® (Stett et al., 2003) platforms with dual-channel microfluidic chips with quartz pipette tips (2.5 μm inner diameter), as described previously (Airini et al., 2019; Mann et al., 2019; Scheel et al., 2014). For manual patch-clamp experiments we used classical setups equipped with

WPC-100 resistive feedback amplifiers (ESF electronic, Göttingen, DE) and pipettes pulled from borosilicate glass capilaries (GC150F-10; Harvard Apparatus, USA) with resistance of 2–3 MΩ in the whole-cell configuration on cells perfused with a home-made solution application system at a flow rate of 100–200 μl/min, as described previously (Airini et al., 2019; Iordache et al., 2016). For hNav1.5 and hKv7.1 experiments, the continuous perfusion flow rate was approximately 1 ml/min and series resistance compensation was 50–80%.

Some experiments on hERG1 channels were performed at physiological temperature (PT: 37°C) using manual patch-clamp and a Peltier-controlled perfusion system similar to that described in (Reid et al., 2001), except for a new microfluidic chamber with lateral walls made of mica instead of glass and an analog instead of a computerized PID (proportional-integrative-derivative) feed-back controller. The flow rate was between 100 and 200 μl/min and the temperature fluctuations of perfused solution were in the range of ±2°C. Other manual patch-clamp experiments at PT were performed on hNav1.5 using a TC01 temperature controller and PH01 perfusion cannula (Multichannel Systems, Reutlingen, DE).

For exploring effects on hERG1 we applied multiple voltage-clamp protocols. In both automated and manual patch-clamp experiments we applied a standard 2-step voltage-clamp protocol, starting from a holding potential of −70 mV, consisting of a 2-s depolarizing step at +40 mV followed by a 2-s step at −50 mV; the peak hERG1 current during this second step was measured relative to the average current during a brief (100 ms) step at −50 mV applied prior to the first depolarizing step.

In manual patch-clamp experiments performed on hERG1 channels at RT one single concentration of drug was tested per experiment. The standard protocol was applied under control conditions in the absence of drug and when the inhibitory effect of drug reached a steady level. In between we applied a modified Milnes protocol (Milnes et al., 2010) with 10-s depolarizing pulses at 0 mV from a holding potential of −80 mV repeated at 25-s intervals. Membrane resistance was monitored with brief (100 ms) pulses to −90 mV applied before the main depolarizing pulses. After testing for the stability of current level at the end of the 10-s depolarizing step in control conditions drug application started. Current traces recorded during this step initially and at steady-state inhibition were used to compute the fractional block (Milnes et al., 2010), and plots of the inverse of time constant of fractional block vs. drug concentration were used for an onset-of-block kinetics analysis to infer the blocking and unblocking rates (Caballero et al., 2004; Wagner et al., 2010). In manual experiments performed at PT we applied 4 increasing concentrations of each tested drug, monitoring the peak hERG current elicited by the standard 2-step votage-clamp protocol applied at 10-s intervals.

In automated patch-clamp experiments the standard voltage-clamp protocol was applied at 10-s intervals with monitoring and continuous plotting of peak hERG1 current, measured relative to the average current during the brief step at −50 mV preceding the main 2-s depolarizing step. After stabilization of peak current amplitude in control conditions a drug was applied consecutively at 4 progressively increasing concentrations under continuous perfusion for 4 min at each concentration to monitor inhibitory effects on peak hERG current, followed by a 5-min wash-out period to assess reversibility of drug inhibition. In a series of experiments we applied a supplementary sequence of 5 voltage-clamp protocols adapted from (Vandenberg et al., 2012) in control conditions and at each drug concentration to explore pharmacological effects on kinetics of hERG current deactivation, inactivation, recovery from inactivation, and voltage dependence of activation and inactivation. All these protocols started from a holding potential of −80 mV. For the deactivation protocol, a 500-ms depolarizing step at +40 mV was followed by 2-s steps between −50 and −160 mV in 10-mV decrements; the current traces during these steps were fitted with double exponential functions to obtain time constants of fast and slow deactivation. For the inactivation protocol, a 500-ms depolarizing step at +40 mV was followed by a brief (25 ms) step at −90 mV for fast recovery from

inactivation, and then by 200-ms depolarizing steps between −80 and + 60 mV in 10-mV increments, during which the time constants of hERG current inactivation were obtained by monoexponential fits. For the recovery-from-inactivation protocol, a 500-ms depolarizing step at +40 mV was followed by 500-ms steps between +40 and −160 mV in 10-mV decrements, during which the time constants of hERG current recovery from inactivation were obtained by monoexponential fits. For the voltage dependence of activation protocol, 5-s depolarizing steps between −70 and + 50 mV in 10-mV increments were followed by a 300-ms step at −50 mV during which the peak hERG current was measured relative to the average level of the first sweep (with prepulse at −70 mV), where no hERG activation occurs; the current values were normalized by dividing peak currents of all sweeps with the highest peak current and plotted against the voltages of the preceding step. For the voltage dependence of inactivation protocol, a 500-ms depolarizing step at +30 mV was followed by brief (30-ms) steps between +30 and −140 mV in 10-mV decrements, during which channels were removed from inactivation to variable degrees, and then by a second 500-ms depolarizing step at +30 mV; the peak tail currents measured at the beginning of this second depolarizing step were plotted against the voltage of the preceding step, fitted with Boltzmann charge-voltage functions, then current values were normalized relative to the upper plateau value of the fit, replotted and refitted with the same function over a range of voltages where deactivation during the 30-ms step exerted negligible effects.

For the cardiac voltage-dependent Na^+ current component hNav1.5 we used a series of voltage-clamp protocols as follows. The protocol for peak and late I_{Na} measurement in the presence of ATX-II started from a holding potential of −120 mV, included a 677-ms preconditioning step at −130mV followed by a 33-ms activation step at −20mV, a 188-ms step at 0 mV and a 88-ms ramp to −110 mV; the repeat interval was 7400 ms. The activation protocol started from a holding potential of −110mV, included a 677-ms preconditioning step at −130 mV followed by a 33-ms activation step between −100 mV and 0 mV in 5-mV increments (21 sweeps); the intersweep interval was 1400 ms. The inactivation protocol started from a holding potential of −110 mV, included a 677-ms preconditioning step at −140 mV up to −40 mV in 5-mV increments (21 sweeps) followed by a 33-ms activation step at −20 mV; the intersweep interval was 1400 ms.

For the slow delayed rectifier K^+ current hKv7.1+hMinK we used a double-step voltage-clamp protocol starting from a holding potential of −110 mV, including a 3300-ms activation step at +20 mV followed by a 4400-ms step at −40mV for measurement of tail current; the repeat interval was 20000 ms.

For the cardiac inward rectifier K^+ current hKir2.1, transfected cells were selected based on green fluorescence via epifluorescence microscopy with blue light excitation and approached by whole-cell patch-clamp. A standard double-ramp voltage protocol, composed of a 2-s ascending ramp from −120 mV to +80 mV followed by a symmetrical descending ramp, starting from a holding potential of −70 mV, was applied repeatedly at 10-s intervals. The current level was measured at −120 mV at the beginning of the ascending ramp. After verifying current level stability in control conditions, 3 μM chloroquine or 10 μM hydroxychloroquine were applied until current inhibition reached a steady value, followed by $BaCl_2$ 1 mM. The current level in $BaCl_2$ was subtracted from previous current measurements to assess the specific hKir2.1 current component.

2.2. Electrophysiology experiments on human induced pluripotent stem cell-derived cardiomyocytes

Ventricular-enriched human induced pluripotent stem cell-derived cardiomyocytes (hiPSC-CM Pluricyte® cardiomyocytes provided by Ncardia) were stored in liquid nitrogen, thawed, plated at high density in 24-well sterile cell culture plates precoated with fibronectin (F1141, Sigma-Aldrich) and cultured in standard conditions (5% CO_2, 37°C) in humidified incubators for up to two weeks, with medium changes every second day, according to manufacturer's instructions. After 2–3 days in culture the cardiomyocytes developed confluent spontaneously contracting monolayers. For experiments cardiomyocytes were dissociated by 7-min treatment with Accutase® at 37°C followed by 3–4 h treatment at the same temperature with 2 mg/ml Collagenase A (11 088 866 001, Roche Diagnostics) in serum-free Iscove's Modified Dulbecco's Medium (IMDM) mixed with standard extracellular solution 1:1. Cells were detached by gentle pipetting, briefly spun in an Eppendorf microcentrifuge, resuspended and plated on 35 mm diameter Petri dishes kept at 37°C for at least 30 min prior to experiments. Manual patch-clamp experiments were performed at room temperature as described above, with the same external and internal solutions, but in the β-escin-perforated whole-cell configuration, using 15–30 μg/ml β-escin added to the pipette solution. After perforation to an access resistance (R_a) of less than 15 MΩ we applied a series of 3 standard voltage-clamp protocols as described previously (Mann et al., 2019) plus the standard double-ramp protocol described above in voltage-clamp mode, and a standard current-clamp protocol with 3 brief current pulses (500 pA, up to 2.5 ms duration, at 3-s intervals). If spontaneous pacemaking was present it was suppressed by applying a faint steady hyperpolarizing current up to 30 pA (Scheel et al., 2014). This sequence of protocols was applied in control conditions, then after 3–5 min from the start of continuous perfusion with 5 μM chloroquine or 10 μM hydroxychloroquine. Voltage-clamp and current-clamp recordings (where ventricular-like action potentials (AP) were present) were analyzed to assess effects of the two compounds on different ion current components and AP parameters.

2.3. Solutions and chemicals

The standard external solution contained (in mM): NaCl 140, KCl 2.5, $MgCl_2$ 2, $CaCl_2$ 2, HEPES 10, D-glucose 10, sucrose 20, pH 7.40 at 25°C titrated with NaOH. $CaCl_2$, $MgCl_2$, glucose and sucrose were added on the day of the experiment from 1 M aqueous stock solutions. The internal (pipette) solution had the following composition (in mM): KCl 140, NaCl 5, $CaCl_2$ 1, $MgCl_2$ 2, EGTA 11, HEPES 10, pH 7.20 at 25°C titrated with KOH. Both solutions were sterile filtered after preparation with 0.22 μm polyvinyl filters (Merck Millipore). For hNav1.5 recordings the external solution contained (in mM): NaCl 140, KCl 4, $CaCl_2$ 5, $MgCl_2$ 1, HEPES 10, pH 7.4 with NaOH, and the internal solution contained (in mM): CsF 60, CsCl 50, NaCl 10, HEPES 10, EGTA 20, pH 7.20 with KOH. For hKv7.1 recordings we used the same external solution as for hNav1.5 and an internal solution containing (in mM): KCl 130, $MgCl_2$ 1, MgATP 5, HEPES 10, EGTA 5, pH 7.20 with KOH. For automated patch-clamp experiments the osmolality of external solution was adjusted to 325 mOsm/kg H_2O and that of internal solution to 290 mOsm/kg H_2O. External solution and deionized water for the automated patch-clamp equipment were degassed overnight by magnetic stirring into bottles connected to a low-grade vacuum pump or by brief boiling in a microwave oven followed by vigorous mechanical shaking to remove air bubbles. For perforated patch-clamp experiments on Pluricyte® hiPSC-CM, β-escin (Sigma E1378) was added freshly to the internal solution on the day of experiment from a 3-mM stock solution in water. Chloroquine sulfate (C1650000) and hydroxychloroquine sulfate (Y0001839) were purchased as European Pharmacopoeia certified reference standard compounds from European Directorate for the Quality of Medicines & HealthCare. Aqueous stock solutions (10 mM) were prepared and stored at −22°C for several weeks. ATX-II (Alomone labs STA-700) was dissolved in external solution at a final concentration of 20 nM. All other chemical reagents were from Sigma-Aldrich or Merck Millipore unless otherwise specified.

2.4. Data analysis

Throughout the paper data are reported as mean ± SD or mean ± SEM, as appropriate, with n indicating the number of cells recorded in

each experimental condition. Statistical significance was tested via Student's *t* tests or one-way ANOVA, their non-parametric variants if normality condition was not met, or regression analysis, using a critical level $\alpha = 0.05$. For experiments on cell lines expressing human cardiac ion channels the selection criteria were a membrane resistance >0.2 GΩ, an access resistance <20 MΩ and a holding current < 100 pA (<300 pA for hKir2.1) at −70 mV. For hiPSC-CM experiments the selection criteria were an access resistance <20 MΩ (in most experiments it decreased <10 MΩ) and an initial holding current < 200 pA (although for most cardiomyocytes it was <100 pA) at −60 mV.

Automated analysis of voltage-clamp and current-clamp recordings in hiPSC-CM was performed as described previously (Mann et al., 2019). Half-inhibitory concentrations (IC50) and Hill coefficients (n_H) for chloroquine and hydroxychloroquine effects on different cardiac ion channels obtained in experiments on cell lines and hiPSC-CM, together with blocking/unblocking rates and activation voltage shifts for hERG1 channels were used to compute proarrhythmogenic risk predictors B_{net} (Mistry, 2018, 2019) and Q_{net} (Dutta et al., 2017). For Q_{net} we used a modified C++ script of the O'Hara-Rudy 2011 model (O'Hara et al., 2011) including the Markov hERG gating model proposed by others (Li et al., 2017b) but with open bound and inactivated open bound states removed, using instead direct experimental estimates of blocking and unblocking rates.

3. Results

3.1. Blocking effects of chloroquine and hydroxychloroquine on hERG1 channels

Both chloroquine and hydroxychloroquine exerted strong inhibitory effects on peak hERG current amplitude measured with the standard manual two-step hERG voltage-clamp protocol (Fig. 1 a,b). During the first 2-s depolarizing step at +40 mV hERG channels open and then inactivate, while during the second 2-s step at −50 mV the channels exit the inactivated state very quickly (in a few milliseconds), giving rise to a specific tail peak hERG current. Measurements of hERG peak current amplitude were done relative to the current level during the 100-ms step at −50 mV preceding the main depolarizing step. Similar results were obtained using the same voltage protocol in automated patch-clamp experiments (CytoPatch™2) in the whole-cell configuration on HEK293T cells stably expressing hERG1. Fig. S1 of Supplemental files illustrates the time lines of corrected peak hERG current measured in automated patch-clamp experiments at 10-s intervals with application of four consecutively increasing concentrations of chloroquine or

hydroxychloroquine, as well as representative current traces recorded in these experiments initially and at each concentration when steady-state inhibition was obtained. Tables S1–S4 of Supplemental files show relative hERG current inhibition by each drug concentration tested in individual automated and manual patch-clamp experiments, as well as average values ± SD. These average values were plotted in dose-response graphs shown in Fig. 1 c,d and were fitted with Hill functions, yielding similar half-inhibitory concentrations (IC50) for each drug in automated vs. manual experiments at RT: for chloroquine IC50 = 1.82 μM (n_H = 1.36) for automated patch-clamp vs. IC50 = 1.85 μM (n_H = 0.90) for manual patch-clamp, and for hydroxychloroquine IC50 = 3.42 μM (n_H = 1.02) for automated patch-clamp vs. IC50 = 4.79 μM (n_H = 0.85) for manual patch-clamp. For chloroquine at PT in manual patch-clamp experiments we obtained IC50 = 1.29 μM (n_H = 1.25) (Fig. 1c and Table S2 of Supplemental files).

In manual patch-clamp experiments only (at RT) we also applied a modified Milnes protocol (Milnes et al., 2010) consisting of 10-s depolarizing steps at 0 mV from a holding potential of −80 mV, repeated at 25-s intervals, to study the onset-of-block kinetics. In Fig. 2 a,b the first traces (marked in red) were recorded initially with this protocol in control conditions, and the subsequent ones in the presence of the blocker, until current inhibition reached a steady-state. By plotting the difference between the initial current and the current in the presence of blocker at steady state (marked in magenta) divided by the former against time we obtained the kinetics of fractional block. The inverse of the monoexponential time constant of fractional block represents the sum of the microscopic blocking and unblocking rates. Therefore by plotting this value at different drug concentrations and applying linear fits we could directly estimate the blocking rates k_B as slopes of these linear fits and the unblocking rates k_{-B} as Y axis intercepts, as shown in Fig. 2 c,d. This method represents the onset-of-block kinetics analysis (Caballero et al., 2004; Wagner et al., 2010). By applying it we obtained for chloroquine k_B = 0.366 μM^{-1}s^{-1}, k_{-B} = 0.108 s^{-1}, and for hydroxychloroquine k_B = 0.213 μM^{-1}s^{-1}, k_{-B} = 0.566 s^{-1}.

We also analyzed the voltage dependence of block induced by the two antimalarial drugs, by measuring the unblocked current following long (5 s) depolarizing steps at different potentials (as shown in Fig. S2 of Supplemental files), considering only those potentials where hERG channel activation is quasicomplete. By fitting these relative peak hERG current vs. voltage plots (illustrated in Fig. 3) with a special Boltzmann charge-voltage function (Amuzescu et al., 2003):

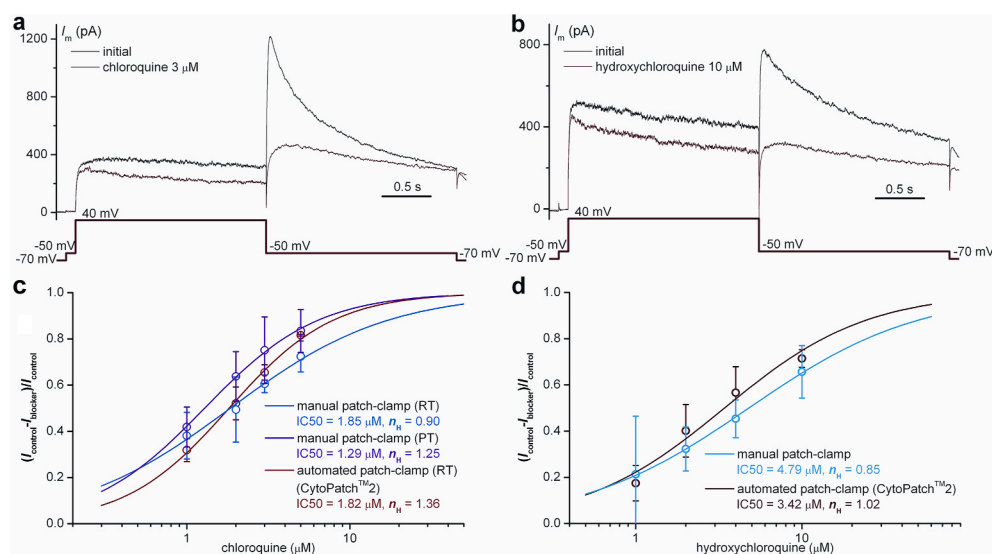$$I_B / I = 1 / (1 + \exp((-\Delta G_{bind} + zF\theta\ V) / RT))$$

Fig. 1. Inhibitory effects of chloroquine and hydroxychloroquine on hERG1 channels. Standard hERG protocol applied to HEK293T cells stably expressing hERG1 approached by manual whole-cell patch-clamp initially and in the presence of chloroquine 3 μM (**a**) or hydroxychloroquine 10 μM (**b**). Dose-response curves for inhibition of peak hERG current elicited with the standard hERG protocol fitted with Hill functions in manual vs. automated patch-clamp experiments for chloroquine (at room temperature-RT, and physiological temperature-PT) (**c**) and hydroxychloroquine (**d**). Data points represent average values and error bars SD of multiple experiments (n = 3–7); individual values are listed in Tables S1–S4 of Supplemental files.
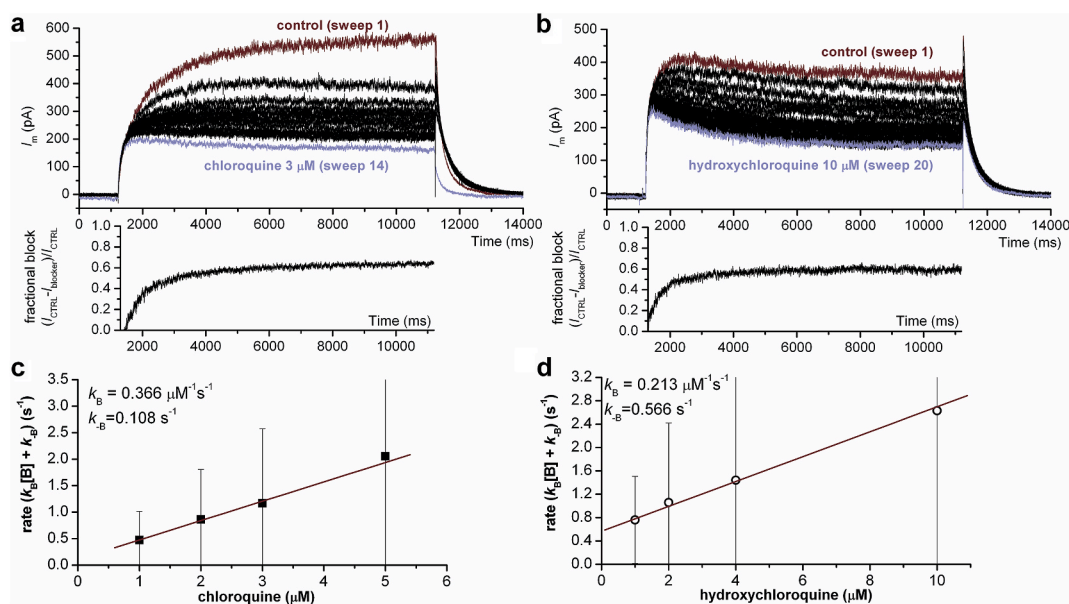
Fig. 2. Inhibitory effects of chloroquine and hydroxychloroquine on hERG1 channels assessed with a Milnes protocol and onset-of-block kinetics analysis. **a,b.** Typical experiments on HEK293T cells stably expressing hERG1 approached by manual whole-cell patch-clamp. A modified Milnes protocol with 10-s depolarizing steps at 25-s intervals was applied: first sweep in control conditions and subsequent sweeps during drug application until current inhibition reached a steday value, allowing computation of the fractional block (lower graphs in **a** and **b**). **c,d.** Onset-of-block kinetics analysis: the inverse of time constant of fractional block was plotted against drug concentration and linear fits provided values of blocking rates k_B (slope) and unblocking rates k_{-B} (Y axis intercepts). Datapoints represent average values and error bars SD of multiple manual patch-clamp experiments ($n = 2$–6) at each concentration.
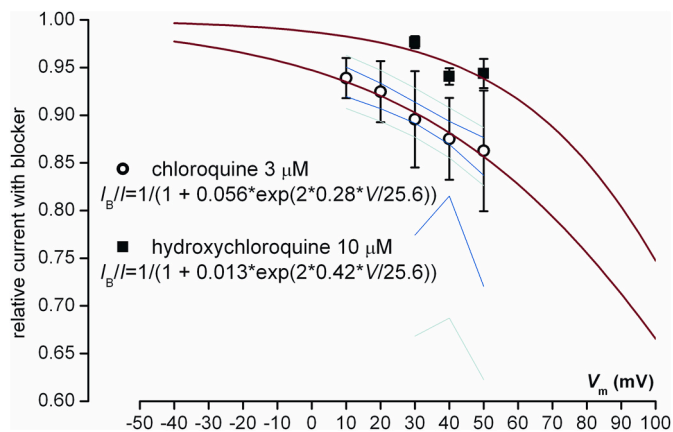

Fig. 3. Voltage dependence of block by chloroquine and hydroxychloroquine of hERG current. Experiments were performed on hERG1 channels stably expressed in HEK293T cells, assessed with the voltage-clamp protocol for voltage dependence of activation in automated patch-clamp experiments. Datapoints represent relative peak hERG current values (average ± SEM) at −50 mV (in the presence of blocker relative to control) over ranges of voltage resulting in complete activation (taken from Fig. 4 a,b) fitted with special Boltzmann charge-voltage functions (details in Supplemental data), yielding relative electrical distances θ of the blocking site in transmembrane electrical field from interior of the membrane amounting to 0.28 for chloroquine and 0.42 for hydroxychloroquine. The blue and cyan lines represent 95% confidence and prediction intervals, respectively. (For interpretation of the references to colour in this figure legend, the reader is referred to the Web version of this article.)

where I_B represents the current amplitude in the presence of the blocker, I the initial current amplitude in control conditions, ΔG_{bind} the Gibbs free energy difference between blocker bound to site and free blocker in solution (neglecting transmembrane electrical field effects), V the transmembrane potential, z the valence of charged blocker molecule expressed in elementary charges (+2 for both chloroquine and hydroxychloroquine at normal pH), RT/F the "quantum" of thermal

energy expressed in electrical potential units (~25.7 mV at 25°C), we could estimate relative electrical distances of the blocking site in transmembrane electrical field (a concept first proposed by Ann M. Woodhull (1973)) from the interior of the membrane θ for the two compounds: 0.28 for chloroquine and 0.42 for hydroxychloroquine (Fig. 3).

3.2. Effects of chloroquine and hydroxychloroquine on hERG1 kinetics and voltage dependence of activation and inactivation

Beyond the main blocking effects, we also explored the influence of the two antimalarials on kinetics and voltage dependence of activation and inactivation of hERG1 channels in automated patch-clamp experiments performed on HEK293T cells with stable hERG1 expression, initially in control conditions and when drug inhibition reached steady-state at each of the 4 concentrations tested. The protocol for voltage dependence of activation (Fig. S2 of Supplemental files) consisted in 5-s depolarizing pulses at various potentials, during which channels opened and subsequently inactivated, followed by a brief pulse at −50 mV that drove the channels rapidly out of inactivation and back in the open state. Thus the peak current amplitude during this step reflects the level of activation at the voltage of the previous step, and by plotting normalized peak current levels vs. voltage of preceding depolarizing step we could obtain the hERG current voltage-dependent activation in control conditions and at different drug concentrations (Fig. 4 a,b).

For studying the voltage dependence of inactivation of hERG1 channels (Fig. S3 of Supplemental files) we applied a 500-ms depolarizing step at +30 mV, followed by 35-ms steps at different hyperpolarized potentials, where hERG channels inactivated during the previous step recovered from inactivation in a voltage-dependent manner; the level of recovery from inactivation was assessed by measuring the peak tail current during the third voltage step at +30 mV. These peak tail current levels are easier to interpret than the peak currents during the preceding hyperpolarizing steps because they are elicited at the same voltage and thus directly reflect levels of hERG conductance activated during the previous step at different voltages. To obtain the voltage-dependent inactivation the peak tail currents were
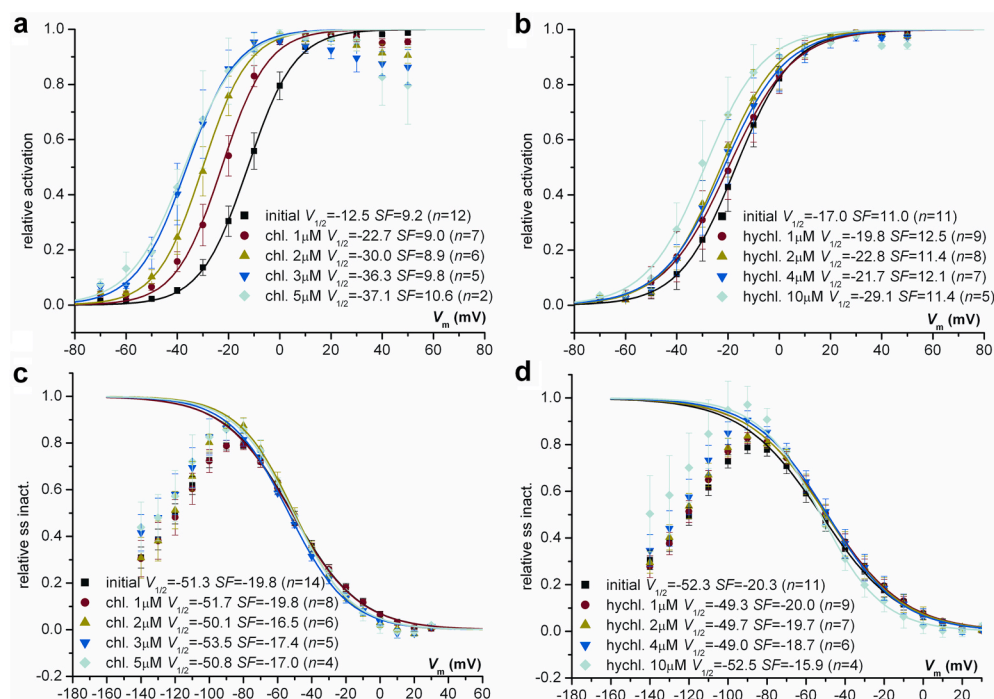
Fig. 4. Effects of chloroquine and hydroxychloroquine on voltage dependence of activation and steady-state inactivation of hERG1 channels stably expressed in HEK293T cells, assessed with specific voltage-clamp protocols in automated patch-clamp experiments. Chloroquine and hydroxychloroquine induce dose-dependent hyperpolarizing shifts of half-activation potentials $V_{1/2}$ without significant changes in slope factors SF (**a,b**), while for steady-state inactivation both $V_{1/2}$ and SF are not significantly changed by drug application (**c, d**). Datapoints represent average values and error bars SEM of multiple automated patch-clamp experiments at each concentration (individual values are listed in Tables S5–S8 of Supplemental files) fitted with Boltzmann charge-voltage functions. $V_{1/2}$ and SF values are in mV; n represents the number of experiments for each average value.

plotted against voltage of preceding step. The plot was fitted with a Boltzmann function, then current values were normalized relative to the plateau current value of this Boltzmann function (Fig. 4 c,d). The data points in Fig. 4 are average values ± SEM of data obtained in multiple experiments in each condition; the individual data are listed in Tables S5–S8 of Supplemental files. Fig. 4 shows that both chloroquine and hydroxychloroquine (although to a lesser extent) shift the sigmoid hERG voltage-dependent activation curves in the hyperpolarizing direction. The voltage-dependent inactivation was not shifted significantly by either compound. In Fig. 5 a,b the average (±SEM) $V_{1/2}$ for activation and inactivation are plotted against concentration of chloroquine and hydroxychloroquine and fitted by linear regression. The slopes of the regression lines were significantly ($p < 0.05$) different from 0 only for activation.

We also examined the effects of the two antimalarials on hERG channels gating kinetics. The hERG deactivation protocol (Fig. S4 of Supplemental files) consisted in a 500-ms depolarizing step at +40 mV followed by long (2-s) steps at different potentials, during which channels were rapidly removed from inactivation and then deactivated. Double-exponential fits of currents recorded during these steps provided fast and slow rates of deactivation, illustrated in Fig. 6 a,b (individual

values provided in Tables S9–S10 of Supplemental files). The fast deactivation rate varies quasiexponentially over the entire range of tested voltages (−50 to −160 mV), while the slow deactivation rate reaches a saturating value of 2–3 s^{-1} at approximately −90 mV.

The voltage protocol for hERG inactivation kinetics (Fig. S5 of Supplemental files) activated the channels with a 500-ms depolarizing step at +40 mV. The subsequent brief step at −90 mV quickly removed channels from inactivation, while the subsequent 200-ms depolarizing steps inactivated them again; inactivation time constants and rates were obtained by monoexponential fits of currents recorded during these steps. The voltage protocol for hERG recovery from inactivation kinetics (Fig. S6 of Supplemental files) is only slightly different from the previous one, lacking the brief intermediate step at −90 mV; hERG channels opened and inactivated during the 500-ms depolarizing step at +40 mV are removed from inactivation during subsequent hyperpolarizing steps, and the rates of recovery from inactivation are obtained from monoexponential fits of currents during this brief recovery stage. Inactivation/recovery form inactivation rates obtained in individual experiments are listed in Tables S11–S12 of Supplemental data, and average (±SEM) values of rates are plotted in Fig. 6 c,d. Theoretically there should be a continuity between the inactivation rates and the
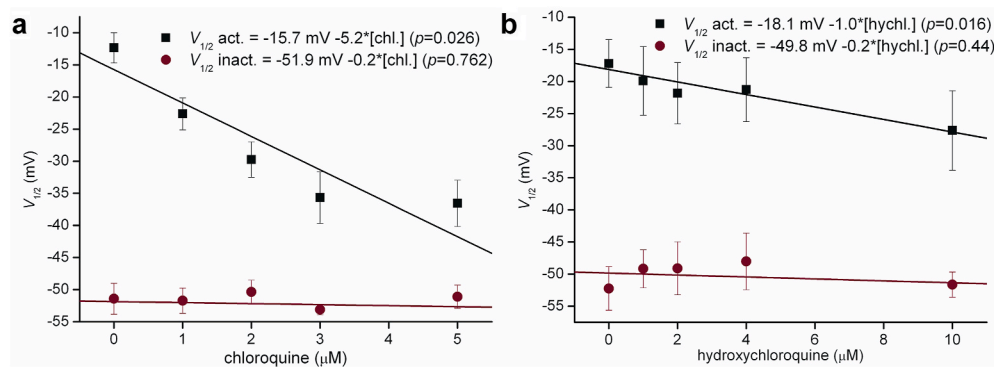
Fig. 5. Concentration-dependent voltage shifts induced by chloroquine and hydroxychloroquine on half-activating and half-inactivating potentials of hERG1 channels stably expressed in HEK293T cells, assessed with specific voltage-clamp protocols in automated patch-clamp experiments. Datapoints represent average values and error bars SEM of activation and inactivation $V_{1/2}$ obtained in multiple automated patch-clamp experiments with chloroquine ($n = 2$–14) (**a**) and hydroxychloroquine ($n = 4$–11) (**b**) at each concentration by fitting with Boltzmann charge-voltage functions (individual values are listed in Tables S5–S8 of Supplemental files). Equations were obtained by linear regression analysis, p representing

statistical significance of correlation coefficients.

Fig. 6. Effects of chloroquine and hydroxy-chloroquine on deactivation, inactivation and recovery from inactivation rates of hERG currents. hERG1 channels stably expressed in HEK293T cells were assessed with specific volta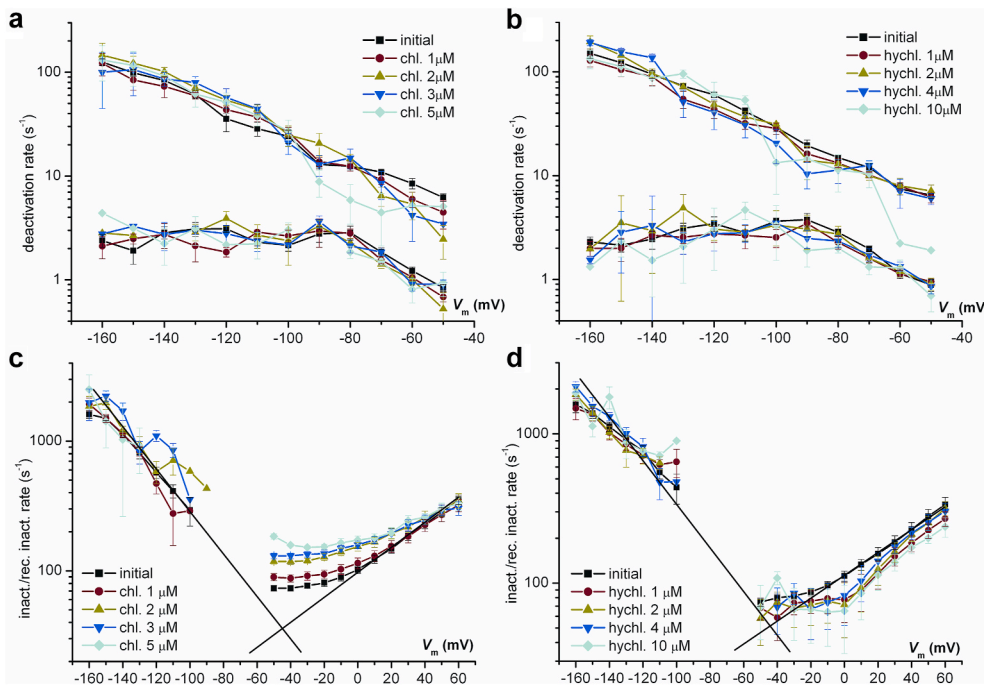ge-clamp protocols in automated patch-clamp experiments. Dose-dependent effects of chloroquine and hydroxychloroquine on fast and slow deactivation rates (**a,b**) and on inactivation and recovery from inactivation rates (**c,d**) assessed at multiple voltages. Datapoints represent average values and error bars SEM of multiple experiments at each concentration ($n = 1$–14) (individual values are listed in Tables S9–S12 of Supplemental files) obtained by fitting individual recordings with double or single exponential functions. The two intersecting lines in graphs **c** and **d** represent estimates of inactivation and recovery from inactivation rates of hERG1 channels in control conditions.

recovery-from-inactivation rates, reflecting the fact that macroscopic time constants measured in these experiments are the inverse of the sum of inactivation and recovery-from-inactivation rates, as described (Vandenberg et al., 2012). Despite the lack of experimental data points at an intermediate potential range (between −50 and −90 mV), our data are compatible with a continuity of plots between the range of inactivation rates and that of recovery-from-inactivation rates. The two intersecting straight lines shown in Fig. 6 c,d represent estimates of voltage-dependent hERG inactivation and recovery-from-inactivation

rates that approach asymptotically the experimental rate plots at extremities. Their point of intersection represents the half-inactivation potential ($V_{1/2}$), with similar values to those found by Boltzmann charge-voltage fits in Fig. 4 c,d.

3.3. Effects of chloroquine and hydroxychloroquine on hNav1.5 peak and late current

Both chloroquine and hydroxychloroquine exerted inhibitory effects
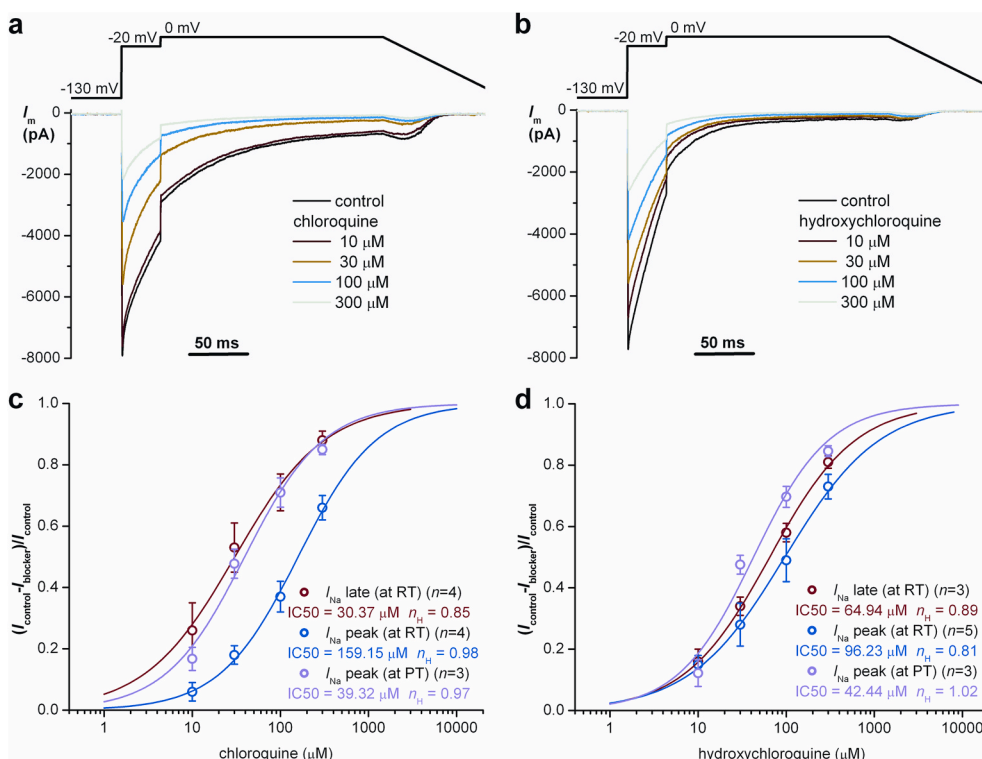
Fig. 7. Inhibitory effects of chloroquine and hydroxychloroquine on hNav1.5 channels in the presence of ATX-II 20 nM. CiPA-compatible voltage protocol for peak and late I_{Na} applied to HEK293T cells stably expressing hNav1.5 in control conditions and in the presence of chloroquine (**a**) or hydroxychloroquine (**b**). Dose-response curves for inhibition of peak and late I_{Na} fitted with Hill functions for chloroquine (**c**) and hydroxychloroquine (**d**). Data points represent average values and error bars SEM of multiple experiments ($n = 4$ for chloroquine, $n = 3$–5 for hydroxychloroquine); individual values are listed in Tables S13 and S14 of Supplemental files.

on peak and late I_{Na} measured in the presence of ATX-II 20 nM in HEK293 cells stably expressing hNav1.5 channels, as shown in Fig. 7 a,b and Tables S13–S14 of Supplemental files. Two measurement points were used to assess inhibitory effects on late Na$^+$ current: immediately before jump from −20 mV to 0 mV (end of step current at −20 mV), and at the end of the voltage step at 0 mV, before the descending voltage ramp (end of tail current at 0 mV). The latter measurement point was preferred and was used further for computation of IC50 values, as shown in Fig. 7 c,d and Tables 1 and 3, yielding the following values:

- I_{Na} peak: IC50 = 159.15 μM (n_H = 0.98) at RT and IC50 = 39.32 μM (n_H = 0.97) at PT for chloroquine, IC50 = 96.23 μM (n_H = 0.81) at RT and IC50 = 42.44 μM (n_H = 1.02) at PT for hydroxychloroquine;
- I_{Na} late: IC50 = 30.37 μM (n_H = 0.85) for chloroquine, IC50 = 64.94 μM (n_H = 0.89) for hydroxychloroquine.

We also explored in separate experiments without ATX-II the effects of the two compounds on voltage dependence of activation and inactivation, and found slight but statistically significant hyperpolarizing shifts (less than 10 mV at highest concentration of drug) of half-inactivating potential $V_{1/2}$, as shown in Figs. S7–S8 and Tables S15–S16 of Supplemental files.

3.4. Effects of chloroquine and hydroxychloroquine on hKv7.1+hMinK current

We explored inhibitory effects of chloroquine and hydroxychloroquine on I_{Ks} via whole-cell experiments on HEK293 cells with inducible expression of hKv7.1+hMinK, using a standard two-step voltage protocol illustrated in Fig. 8 a,b. The plateau I_{Ks} level measured at the end of the first depolarizing step at +20 mV was only slightly inhibited by the highest concentrations of drug applied (100 μM), as shown in Fig. 8 c,d and Tables S17–S18 of Supplemental files.

3.5. Effects of chloroquine and hydroxychloroquine on hKir2.1 current

HEK293T cells expressing hKir2.1 channels were selected based on eGFP fluorescence (the eGFP gene was present together with the hKir2.1 gene KCNJ2 on the same plasmid) and approached by whole-cell manual patch-clamp. The standard double-ramp voltage-clamp protocol (ascending ramp −120 mV to +80 mV in 2 s with symmetrical descending ramp) was applied repeatedly at 10-s intervals and the current level at −120 mV at the beginning of the ascending ramp was monitored. After verifying current stability in control conditions, chloroquine 3 μM or hydroxychloroquine 10 μM were applied until current inhibition reached steady values, followed by BaCl$_2$ 1 mM, a strong blocker of Kir2.1 channels. Fig. 9 a,b illustrates I–V plots of current traces recorded in typical experiments initially, under drug application

at steady inhibition, and during final application of BaCl$_2$ (only the ascending voltage ramp is shown), while Fig. 9 c,d illustrates the time course of current inhibition. Current levels recorded in individual experiments are listed in Tables S19–S20 of Supplemental files. Average (±SD) steady inhibition of Kir2.1 current amounted to 33.85 ± 4.04% for 3 μM chloroquine and 25.46 ± 8.88% for 10 μM hydroxychloroquine, resulting in estimated IC50 for hKir2.1 channels of 5.86 μM for chloroquine and 29.28 μM for hydroxychloroquine, respectively (Table 1).

3.6. Effects of chloroquine and hydroxychloroquine on multiple ion currents and APs recorded in Pluricyte® ventricular hiPSC-CM

Experiments on ventricular hiPSC-CM commercial preparations (Pluricyte® cardiomyocytes from Ncardia) were performed by manual patch-clamp in the β-escin-perforated whole-cell patch-clamp configuration (Mann et al., 2019), as described in the Methods section. By applying the sequence of 3 standard voltage-clamp protocols (Mann et al., 2019) in control conditions initially and at 3–5 min since start of drug application we could assess specific inhibitory effects of the two compounds on peak voltage-dependent Na$^+$ current (I_{Na}), peak L-type Ca^{2+} current (I_{CaL}), peak hERG current (I_{Kr}), and steady funny current (I_f). Furthermore, applying a standard current-clamp protocol we could estimate via automated analysis changes in parameters of externally paced APs induced by the two compounds. Tables S21–S30 of Supplemental files list drug-induced changes in ion currents and AP parameters obtained in individual experiments, and Fig. 10 illustrates changes in peak I_{Na}, peak I_{CaL}, and peak I_{Kr}, as well as changes in AP shape induced by chloroquine or hydroxychloroquine in typical experiments. Chloroquine (5 μM) produced an average (±SD) peak I_{Na} inhibition to 90 ± 12% of control values (i.e. a 10% average inhibition), corresponding to an IC50 of 45 μM, average peak I_{CaL} inhibition to 86 ± 9% of control values, corresponding to an IC50 of 30.7 μM, and an average peak I_{Kr} inhibition by 62.78 ± 11.12% (to 37.22% of control values). Hydroxychloroquine (10 μM) produced an average (±SD) peak I_{Na} inhibition to 84 ± 16% of control values, corresponding to an IC50 of 52.5 μM, a peak I_{CaL} inhibition to 90 ± 12% of control values, corresponding to an IC50 of 90 μM, and a peak I_{Kr} inhibition by 70.65 ± 18.14% (to 29.35% of control values). Both compounds failed to elicit any significant effect on steady I_f amplitudes at the concentrations tested. In current-clamp recordings, 5 μM chloroquine produced on average only a mild prolongation of APD90 of externally paced APs (average APD90 104.1 ± 32.7% with chloroquine relative to control). Hydroxychloroquine 10 μM produced an average APD90 prolongation to 119.2 ± 82.6% of control values.

3.7. Estimation of proarrhythmogenic risk predictors B_{net} and Q_{net} for chloroquine and hydroxychloroquine

The IC50 values for chloroquine and hydroxychloroquine inhibition of several human cardiac ion channels obtained in this study (plus a few data from literature), as well as maximal effective free therapeutic plasma concentrations (*EFTPC* or C_{max}) for the two compounds extracted also from literature are summarized in Table 1. With these pharmacological inhibition data and C_{max} values we computed the proarrhythmogenic risk predictor B_{net} (Mistry, 2018, 2019) using the formula:

$$B_{net} = \sum_{i=1}^{n} R_i - \sum_{j=1}^{m} D_j$$

where ΣR_i and ΣD_j represent the sums of relative inhibitions of repolarizing and depolarizing cardiac ion currents, defined using C_{max} (*EFTPC*) values:

Relative inhibition (R_i or D_j) = 1 / (1 + *IC50* / C_{max})

The B_{net} values obtained via this method (B_{net} = 0.09116 for chloroquine, B_{net} = 0.09176 for hydroxychloroquine) were compared with

Table 1
Estimated chloroquine and hydroxychloroquine C_{max} and half-inhibitory concentrations (IC50) for I_{Na} (peak and late), I_{CaL}, I_{to}, I_{Kr}, I_{Ks}, I_{K1}.

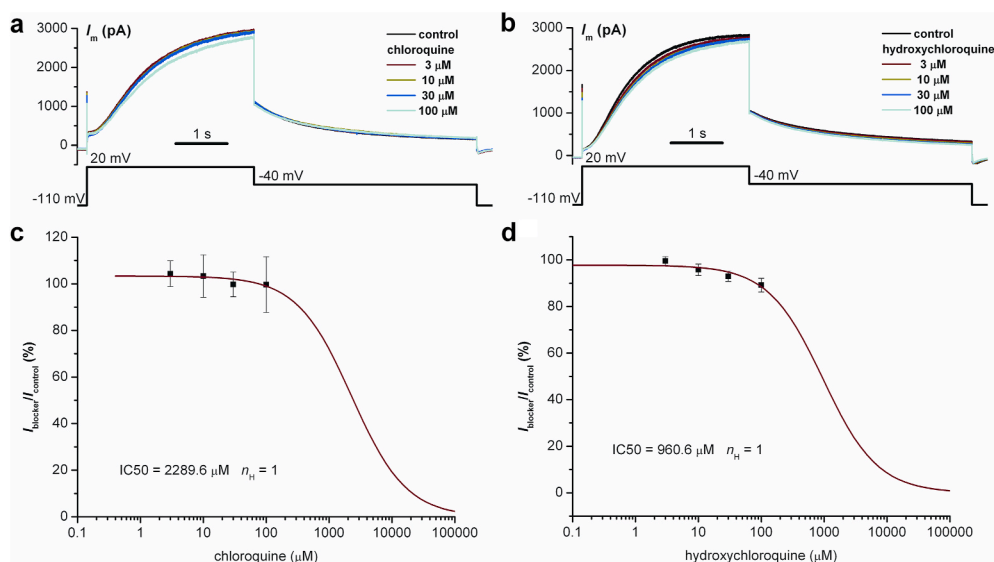|	Chloroquine		Hydroxychloroquine	
	Value (μM)	source	Value (μM)	Source
C_{max}	0.41	Borsini et al. (2012)	0.495 (215 ng/ml)	Yao et al. (2020)
$I_{Na\ peak}$ IC50	159	own data	96.2	own data
$I_{Na\ late}$ IC50	30.4	own data	64.9	own data
I_{CaL} IC50	30.7	own data	90	own data
I_{to} IC50	4600	Wagner et al. (2010)	4600	analogy with chloroquine
I_{Kr} IC50	1.82	own data	3.42	own data
I_{Ks} IC50	>100	own data	>100	own data
I_{K1} IC50	5.86	own data	29.28	own data

Fig. 8. Inhibitory effects of chloroquine and hydroxychloroquine on hKv7.1+hMinK channels. A double-step voltage protocol was applied to HEK293T cells stably expressing hNav1.5 in control conditions and in the presence of chloroquine (**a**) or hydroxychloroquine (**b**). Dose-response curves for I_{Ks} inhibition were fitted with Hill functions for chloroquine (**c**) and hydroxychloroquine (**d**). Data points represent average values and error bars SEM of multiple experiments ($n = 3$); individual values are listed in Tables S17 and S18 of Supplemental files.
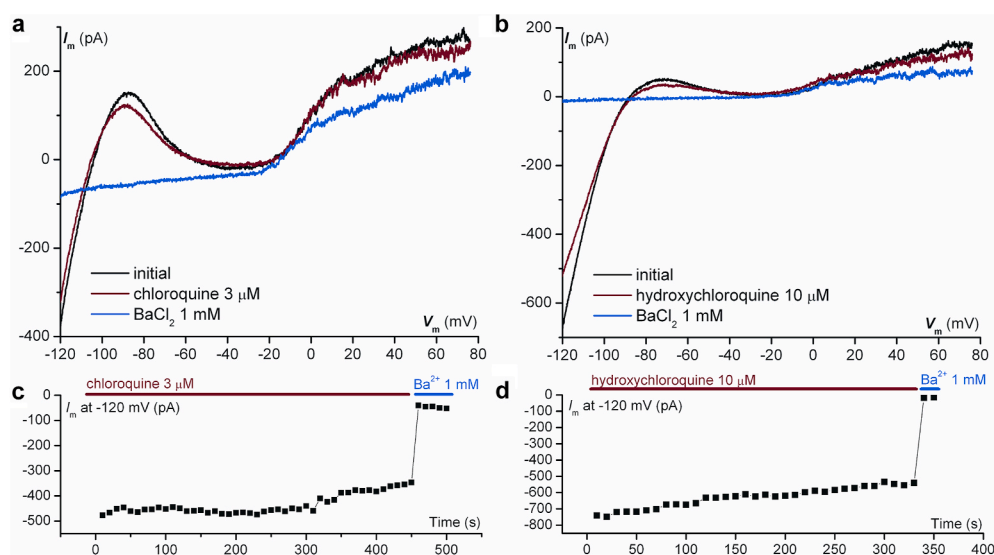

Fig. 9. Effects of chloroquine and hydroxychloroquine on cardiac inward rectifier K$^+$ channels hKir2.1 transiently expressed in HEK293T cells. Current inhibition exerted by prolonged application of chloroquine 3 μM (**a**) and hydroxychloroquine 10 μM (**b**) (red traces) vs. initial recordings (black traces) and traces with complete block of hKir2.1 channels by application of BaCl$_2$ 1 mM (blue traces). The graphs represent current recordings during the ascending ramp of the double-ramp voltage-clamp protocol, with voltage variation from −120 mV to +80 mV in 2 s. Lower panels show time course of inhibition by chloroquine (**c**) and hydroxychloroquine (**d**) and final suppression by BaCl$_2$ 1 mM of current measured at −120 mV at the beginning of the ascending ramp. (For interpretation of the references to colour in this figure legend, the reader is referred to the Web version of this article.)

B_{net} values of 12 compounds belonging to different proarrhythmogenic risk groups (Dutta et al., 2017) (Table 2) and were placed in the intermediate risk group.

We proceeded further to compute another relevant proarrhythmogenic risk predictor, Q_{net} (Dutta et al., 2017). For this purpose we used for numeric integration simulations an O'Hara-Rudy human ventricular cardiomyocyte electrophysiology and Ca^{2+} cycling model (O'Hara et al., 2011) with subendocardial cardiomyocyte parameter set (cell type = 0), including a Markov gating model for hERG as defined by (Li et al., 2017b), but we simplified the pharmacodynamic component of this Markov model by removing the open bound (O*) and inactivated open bound (IO*) states and connecting directly the blocked state (C*) to the open (O) and inactivated (I) state by experimentally-derived blocking and unblocking rates (Fig. S9 of Supplemental files). The reasons for this simplifying change are multiple. First, we wanted to make use of the hERG blocking and unblocking rates for chloroquine and hydroxychlorquine estimated directly from experiments by onset-of-block kinetics analysis. Second, although the open bound and inactivated open bound states exist in reality beyond any doubt, corresponding to hERG channel conformations where the blocker molecule entered the inner vestibule without occupying the final blocking

position and occluding the ion permeation pathway, in practice they are extremely difficult to distinguish from the corresponding non-bound states, featuring the same single-channel levels of conductance. The distinction based on drug trapping effects and changes in relative fractional block at consecutive applications of the Milnes protocol is also tricky because the pharmacokinetics of drug penetration into the cell is variable from one cell to another and rather impredictable, as shown by own experiments (Fig. 2 a,b), and may interfere with the drug trapping effect. In order to use this simplified Markov model for the standard CiPA drugs, we introduced for them compound blocking rates $E_{max}(D)$ *Kt, assuming that only the fraction $E_{max}(D)$ of channels in the open or inactivated state is available for drug block. Simulations with this modified cardiomyocyte electrophysiology and pharmacology model (C++ script available at https://github.com/bamuzesc/Qnet-for-CiPA. git, https://zenodo.org/record/5615548#.YXvbQ7hyGSp) were run for chloroquine, hydroxychloroquine and the standard CiPA compounds at concentrations from 1x C_{max} to 25x C_{max}. At each concentration we ran 1000 2-s pacing cycles and collected Q_{net} values for the last 10 cycles. For chloroquine and hydroxychloroquine we ran the simulations both with and without including the drug-induced voltage shifts in half-activation potential (approximated by the linear fits shown in Fig. 5
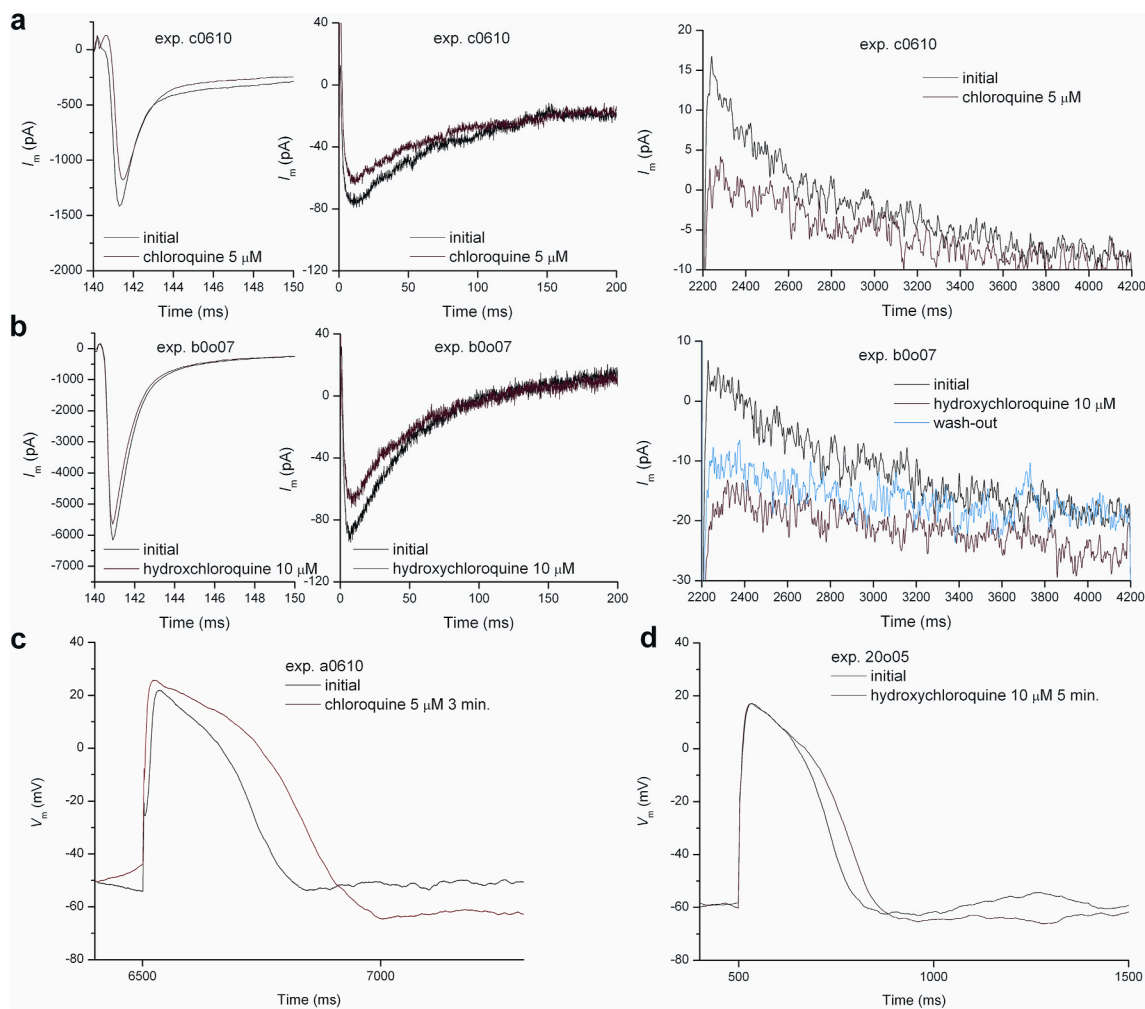
Fig. 10. Effects of chloroquine and hydroxychloroquine on individual ion current components and APs recorded in Pluricyte® hiPSC-derived cardiomyocytes. Inhibitory effects of chloroquine 5 μM (**a**) and hydroxychloroquine 10 μM (**b**) on peak I_{Na}, peak I_{CaL}, and peak I_{Kr} recorded with the three standard voltage-clamp protocols described in Mann et al., (2019). Prolongation of externally paced APs recorded in current-clamp mode induced by chloroquine 5 μM (**c**) and hydroxy-chloroquine 10 μM (**d**).

Table 2
Computation of sum of relative inhibitions of repolarizing (ΣR_i) and depolarizing (ΣD_j) cardiac ion currents used to estimate proarrhythmogenic risk predictor B_{net} (Mistry, 2018, 2019) for chloroquine and hydroxychloroquine compared to the standard 12-compounds panel used by Dutta et al., (2017) (Dutta et al., 2017) for defining Q_{net}.

Compound	C_{max} (nM)	ΣR_i	ΣD_j	B_{net}
Low proarrhythmogenic risk				
Mexiletine	4129	0.12513	0.41306	−0.28793
Diltiazem	122	0.00919	0.52779	−0.5186
Ranolazine	1948.2	0.19068	0.22572	−0.03504
Verapamil	81	0.21951	0.29782	−0.0783
Intermediate proarrhythmogenic risk				
Chlorpromazine	38	0.03929	0.02527	0.01402
Ondansetron	139	0.09541	0.01573	0.07968
Hydroxychloroquine	495	0.12654	0.03478	0.09176
Chloroquine	410	0.18561	0.09445	0.09116
Terfenadine	4	0.14816	0.00671	0.14145
Cisapride	2.6	0.20474	8.85E-05	0.20465
High proarrhythmogenic risk				
Sotalol	14690	0.11759	0.00703	0.11056
Bepridil	33	0.40142	0.04063	0.36078
Dofetilide	2	0.38601	0.0179	0.36811
Quinidine	3237	1.24681	0.52288	0.72393

a,b) applied to the voltage dependency of all opening and closing rates included in the hERG Markov model, but including half-activation potential shifts produced only small effects on simulated APs and Q_{net} values (Tables S31–S32 of Supplemental files). We also performed simulations with the modified O'Hara-Rudy model (Li et al., 2017b) incorporated in the Nottingham AP portal (https://cardiac.nottingham.ac.uk) (Williams and Mirams, 2015), which uses an IC50-based estimation of hERG inhibition by drugs, and independently with our own script of the modified O'Hara-Rudy model (Li et al., 2017b) without pharmacodynamic component and using a hERG open-state probability weighted by hERG IC50 values for I_{Kr} computation [$I_{Kr} = G_{Kr}\cdot\sqrt{[K^+]_o/5.4}\cdot IKrO\cdot(V - E_K)/(1 + nC_{max}/IC50)$]. In both series of simulations we used the experimental pharmacological inhibition data for chloroquine and hydroxychloroquine exposed in Table 1, performing 1000 2-s simulation cycles for drug concentrations in the range of 0–25x C_{max}. The results of these IC50-based hERG inhibition simulations were very similar, as shown in Tables S31–S32 and Figs. S10–S11. However, using the experimentally measured hERG blocking/unblocking rate modeling approach resulted in higher Q_{net} values, which became similar to the hERG IC50-based predicted Q_{net} values for chloroquine only at high concentrations (>20x C_{max}, Fig. S10). Increasing the hERG blocking rate (k_B) by 3x for chloroquine resulted in Q_{net} values similar to those of hERG IC50-based simulations at low concentrations (1–4 x C_{max}, Fig. S10), while increasing hERG k_B by 4.8x for hydroxychloroquine

Table 3

Estimated half-inhibitory concentrations (IC50) of chloroquine and hydroxychloroquine for different cardiac ion currents from own experiments compared to data retrieved from the literature (RT - room temperature, PT - physiological temperature, SAN - sino-atrial node).

Cardiac ion current	IC50 (µM)		Preparation	Ref.
	own data	Literature		
Chloroquine				
I_{Kr}	1.82 at RT	0.96 at RT	HEK293	Borsini et al. (2012)
	1.29 at PT	1.03 at PT	CHO	Delaunois et al. (2021)
		1.47 at PT	CHO	TeBay et al. (2021)
		1.6 at PT (65% block at 3 µM)	cat Purkinje fibers	Sánchez-Chapula et al. (2001)
		2.5 at RT	HEK293	Traebert et al. (2004)
		7.77	CHO	Jordaan et al. (2021)
		8.4	*Xenopus laevis* oocytes	Sánchez-Chapula et al. (2002)
I_{Ks}	>100	>80.9 (11% block at 10 µM)	cat Purkinje fibers	Sánchez-Chapula et al. (2001)
		115 (8% block at 10 µM)	human atrial myocytes	Borsini et al. (2012)
		>300	CHO	Delaunois et al. (2021)
I_{K1}	5.86	0.35 (74% block at 1 µM)	cat Purkinje fibers	Sánchez-Chapula et al. (2001)
		1.2	HEK293	Noujaim et al. (2011)
		4.98	CHO	Delaunois et al. (2021)
I_{Na} peak	159.15 at RT	8.48	HEK293	Jordaan et al. (2021)
	39.32 at PT	12.2 (45% block at 10 µM)	cat Purkinje fibers	Sánchez-Chapula et al. (2001)
		40.4 (42.6% block at 30 µM)	human atrial myocytes	Borsini et al. (2012)
		64.2 at RT, 13.95 at PT	CHO	Delaunois et al. (2021)
I_{Na} late	30.37	109.2 at RT, 11.6 at PT	CHO	Delaunois et al. (2021)
I_{CaL}	30.7	3.05	HEK293	Jordaan et al. (2021)
		17.95 at RT	CHO	Delaunois et al. (2021)
		21.25 (32% block at 10 µM)	cat Purkinje fibers	Sánchez-Chapula et al. (2001)
I_{to}	–	>240 (4% block at 10 µM)	cat Purkinje fibers	Sánchez-Chapula et al. (2001)
		>300	CHO	Delaunois et al. (2021)
		4600	rat ventricular myocytes	Wagner et al. (2010)
I_f	>161.7	227.95 at RT	HEK293	Delaunois et al. (2021)
hydroxychloroquine				
I_{Kr}	3.42 at RT	3.78 at PT	CHO	TeBay et al. (2021)
		5.6 at PT (35% block at 3 µM)	guinea pig SAN cells	Capel et al. (2015)
		6.97 at RT	CHO	Delaunois et al. (2021)
		2.66 at PT		
		9.7	CHO	Jordaan et al. (2021)
I_{Ks}	>100	>300 at RT	CHO	Delaunois et al. (2021)
I_{K1}	29.28	44.15 at RT	CHO	Delaunois et al. (2021)
I_{Na} peak	96.23 at RT	44.15 at RT, 16.99 at PT	CHO	Delaunois et al. (2021)
	42.44 at PT	>300	HEK293	Jordaan et al. (2021)
I_{Na} late	64.94	92.87 at RT 21.43 at PT	CHO	Delaunois et al. (2021)
I_{CaL}	90	7.64	HEK293	Jordaan et al. (2021)
		22 at PT (12% block at 3 µM)	guinea pig SAN cells	Capel et al. (2015)
		66.29 at RT	CHO	Delaunois et al. (2021)
I_{to}	–	>300 at RT	CHO	Delaunois et al. (2021)
I_f	>990	22 at PT (12% block at 3 µM)	guinea pig SAN cells	Capel et al. (2015)
		372.3 at RT, >300 at PT	HEK293	Delaunois et al. (2021)

reached IC50-based Q_{net} predictions at 20–25 x C_{max} (Fig. S11). Complex pharmacological effects of the two compounds on AP shape obtained in different types of simulations are illustrated in Figs. S12–S17.

Q_{net} values for the two antimalarial compounds (using experimental hERG blocking/unblocking rate estimates, including drug-induced activation voltage shifts), together with values for the standard 12-compounds panel (CiPA training set) used by (Li et al., 2017b) and (Dutta et al., 2017), as well as for other 16 compounds included in a CiPA validation set (Han et al., 2020; Li et al., 2020) (with inhibition data retrieved from https://github.com/FDA/CiPA/tree/Lab_Specific_Validation_Calibration_2020/and https://github.com/FDA/CiPA/blob/Lab_Specific_Validation_Calibration_2020/), for concentrations ranging from 1 x C_{max} to 25 x C_{max}, are illustrated in Fig. 11a and b. These simulations yielded the following values:

- chloroquine: Q_{net} at 4 x C_{max}: 62.81 nC/µF
- hydroxychloroquine: Q_{net} at 4 x C_{max}: 65.84 nC/µF

placing both compounds in the intermediate proarrhythmogenic risk group. Fig. 12 shows correlation between B_{net} and Q_{net} at 4 x C_{max} for chloroquine, hydroxychloroquine and the standard 12-compound panel used previously (Dutta et al., 2017; Li et al., 2017b).

4. Discussion

In the present study we characterized inhibitory effects of chloroquine and hydroxychloroquine on human cardiac ion channels in heterologous expression systems and hiPSC-CM preparations. Assessment of inhibitory potency of these two compounds yielded IC50 values largely similar with previous reports (Table 3). Disparity with literature was observed for hKir2.1 (Sánchez-Chapula et al., 2001), for HCN (Capel et al., 2015), and for Cav1.2 (Jordaan et al., 2021). These differences may be due to influence on IC50 of experimental protocol and measurement method (Gomis-Tena et al., 2020), or variable enantiomer composition (Ducharme and Farinotti, 1996; Lentini et al., 2020). IC50 values for multiple cardiac ion currents decrease with temperature increase to 37°C (Delaunois et al., 2021), although further rise to 42°C reduces hERG inhibition (TeBay et al., 2021).

hERG inhibitory effects of the two 4-aminoquinoline drugs play significant roles for their proarrhythmogenic risk. Using a modified Milnes protocol (Milnes et al., 2010) to assess fractional block and the onset-of-block kinetics analysis (Caballero et al., 2004; Wagner et al., 2010) we obtained direct estimates of hERG channels blocking and unblocking rates. The relative electrical distances θ of blocking site from interior found by us are smaller than the value of 0.57 that can be
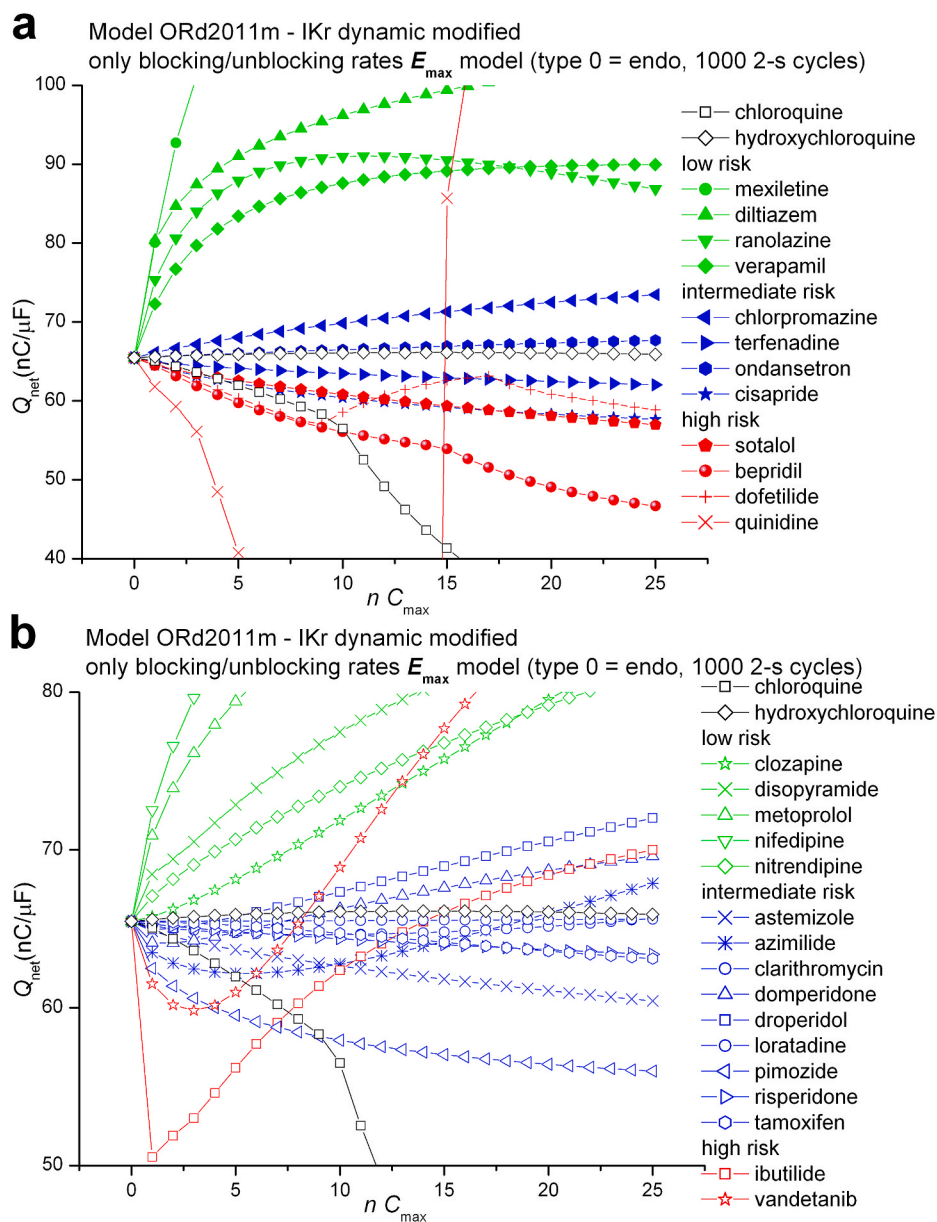
Fig. 11. Q_{net} values at concentrations between 1x and 25x C_{max} computed with a modified O'Hara et al., 2011 model with the simplified hERG gating Markov model proposed by us for chloroquine, hydroxychloroquine and: (**a**) the standard 12-compounds set used by Li et al. 2017 and Dutta et al., (2017) (the CiPA training set); (**b**) a supplementary 16-compounds set used by Han et al., (2020) and Li et al., (2020) (the CiPA validation set).

computed for chloroquine from data reported by others (Sánchez-Chapula et al., 2002).

Another result of our study is the hyperpolarizing shift in voltage dependence of hERG activation induced by chloroquine/hydroxy-chloroquine, while the voltage dependence of inactivation is not changed (Figs. 3 and 4 and Tables S5–S8 of Supplemental files). Similar hyperpolarizing shifts of hERG channels half-activation potential were reported for almokalant and dofetilide in studies on dissociated rabbit or guinea pig ventricular myocytes performed by Prof. Edward Carmeliet in the early 1990s (Carmeliet, 1992, 1993). Since then it was clear that the shift is genuine, not a result of reversible state-dependent block, that it can counteract blocking effects by increasing the fraction of open channels, and that it may result from drug binding to a secondary site distinct from the blocking site, with faster accessibility and different affinity (Carmeliet, 1993). This general property of drugs to exert hyperpolarizing shifts in voltage-dependent hERG activation in addition to block was named facilitation by Perry, Sanguinetti and Mitcheson

(Perry et al., 2010). A helical wheel analysis of differential effects on hERG block and facilitation of S6 point mutants (Hosaka et al., 2007), together with the assumption that a hyperpolarizing shift in voltage dependence of hERG activation requires actions exerted before channel opening, leads to the conclusion that facilitation involves drug binding to secondary sites on hERG channels, distinct from the blocking site, involving S6 residues not facing the inner cavity (Gessner et al., 2010).

Drug trapping in the inner cavity by hERG channel closure has been also described (Carmeliet, 1993). Mitcheson et al. demonstrated the trapping mechanism using a hyperpolarization-activated hERG point-mutant (D540K) where MK-499 block was removed at −160 mV (Mitcheson et al., 2000). Using the Milnes protocol (Milnes et al., 2010), Windley et al. assessed the drug trapping mechanism for several hERG blockers (Windley et al., 2017). However, with a unique long-depolarization step protocol it is virtually impossible to distinguish real drug trapping (by channel closure) from apparent drug trapping by slow dissociation from a high-affinity open/inactivated blocked state
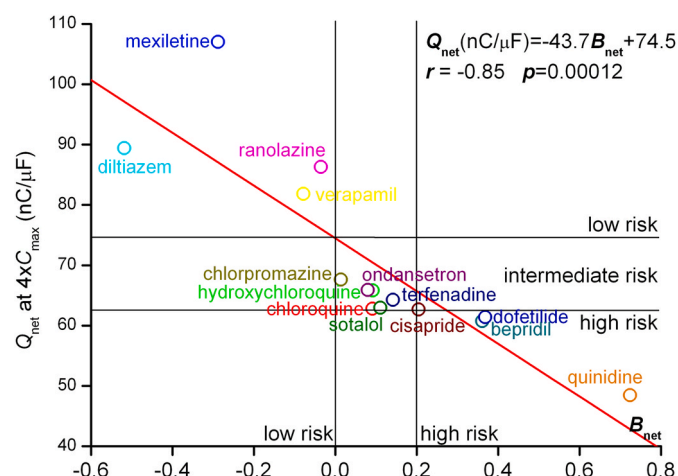
Fig. 12. Correlation between B_{net} and Q_{net} values at 4x C_{max} for chloroquine, hydroxychloroquine and the standard 12-compounds set used by Li et al. 2017 and Dutta et al., (2017). The linear regression equation, correlation coefficient and its statistical significance are shown in insert. Both predictors classify fairly well compounds into low, intermediate and high proarrhythmogenic risk groups (demarcation lines shown on graph).

(so-called virtual drug-trapping) or from pharmacokinetic effects in cell lines featuring temperature-dependent transmembrane drug transporters (Windley et al., 2017, 2018). In our experiments the protocol used precluded reliable assessment of drug trapping, although we presume it is present for both drugs. Beyond trapping, the differences between IC50 and apparent blocking K_D could be influenced by the above-mentioned hyperpolarizing shifts in voltage dependence of activation/deactivation rates, given that blocking rates (at least at room temperature) for fast blockers are limited by hERG channel activation rates (Windley et al., 2017).

We found (Fig. 6 and Tables S9–S12 of Supplemental files) that both compounds influenced hERG deactivation, inactivation and recovery-from-inactivation rates. Most striking were effects of chloroquine on deactivation rates at less negative potentials (e.g. −50 mV), where a dose-dependent slow-down of deactivation could be evidenced. The continuity of activation and recovery-from-inactivation in rate vs. voltage plots (Fig. 6 c,d) is in agreement with previous reports (Vandenberg et al., 2012). Although type 1 and 2 hERG activators have been shown to attenuate inactivation (Perry et al., 2009), and other hERG blockers seem to bind with higher affinity to inactivated channels (Perrin et al., 2008), our data do not support such effects. Halofantrine, a chloroquine analogue, was found to bind to inactivation-deficient point-mutant hERG channels (G628C/S631C) with similar affinity compared to wild-type channels (Sánchez-Chapula et al., 2004).

Inhibitory effects of chloroquine and hydroxychloroquine on peak and late I_{Na} as well as lack of effect on I_{Ks} found in our study are in good agreement with previous reports (Borsini et al., 2012; Delaunois et al., 2021; Jordaan et al., 2021; Sánchez-Chapula et al., 2001).

Inhibitory effects of chloroquine and hydroxychloroquine on cardiac inward rectifier K^+ channels Kir2.1 have been described previously, with different affinities depending on preparation and experimental protocol (Delaunois et al., 2021; Noujaim et al., 2011; Rodríguez-Menchaca et al., 2008; Sánchez-Chapula et al., 2001). The proposed mechanism is direct pore block by interaction with several negatively charged residues lining the permeation pathway, including E224, D255, D259, E299 (Noujaim et al., 2011; Rodríguez-Menchaca et al., 2008).

Experiments on Pluricyte® hiPSC-CM via β-escin-perforated patch-clamp and a series of voltage-clamp and current-clamp protocols established previously (Mann et al., 2019) allowed us to estimate inhibitory effects of the two compounds on multiple ion current components including I_{Na} peak, I_{CaL} peak, I_{Kr} and I_f in physiological

conditions, without adding high-potency specific blockers for pharmacological isolation of these ion current components. For I_{Kr} the estimated IC50 values (2.96 μM for chloroquine and 4.15 μM for hydroxychloroquine) were largely similar to those yielded by both automated and manual patch-clamp experiments on hERG1-expressing HEK293 cells. Although with the currently applied protocol we could measure only the total delayed rectifier K^+ current, representing a mixture of I_{Kr} and I_{Ks}, usually I_{Kr} is the main component, while I_{Ks} activation requires β-adrenergic stimulation. In our experimental conditions we could elicit externally-triggered APs in over 40% of the hiPSC-CM (Amuzescu et al., 2021), and most of them were ventricular-like (Tables S29–S30 of Supplemental files), but in some cases we had to apply steady external hyperpolarizing currents up to 30 pA to suppress spontaneous pacemaking (Scheel et al., 2014). APD prolongation by chloroquine/hydroxychloroquine in individual experiments is consistent with that reported by others (Borsini et al., 2012; Capel et al., 2015; Filgueiras-Rama et al., 2012; Sánchez-Chapula et al., 2001) and with QT$_c$ prolongation induced by chloroquine in clinical trials (Becker et al., 2021; Cardiac Arrhythmia Suppression Trial (CAST) Investigators, 1989; Cook et al., 2006; Vicente et al., 2019).

Both B_{net} (Mistry, 2018, 2019) and Q_{net} (Dutta et al., 2017; Li et al., 2017b) are reliable proarrhythmogenic risk predictors. Our study proved statistically significant correlation for chloroquine/hydroxychloroquine and the 12-compound panel used by (Li et al., 2017b). Q_{net} values found by us for the two antimalarials (Table S31 of Supplemental files) are similar to those reported by (Delaunois et al., 2021; Whittaker et al., 2021), along with APD-prolongation and EAD-induction effects found in other simulation studies (Montnach et al., 2021; Varshneya et al., 2021). Although Q_{net} provides an in-depth mechanistic interpretation of proarrhythmogenic effects (Parikh et al., 2019), we found that the method requires supplementary precautions and avoiding simulated APs that actually feature EADs.

Clinical studies evidenced significant QT prolongation by chloroquine and hydroxychloroquine (Borba et al., 2020; Chorin et al., 2020; Roden et al., 2020; Vicente et al., 2019) and increased risk of arrhythmias (ventricular tachycardia/fibrillation, torsades-de-pointes, cardiac arrests) (Gérard et al., 2020; Grandvuillemin et al., 2021; Roden et al., 2020; Tleyjeh et al., 2020), particularly at high doses and during hypokaliemia (TeBay et al., 2021). Although initial *in vitro* efficiency results (Wang et al., 2020) and non-randomized clinical trials suggested effectiveness against coronavirus-induced cytokine storm (Gao et al., 2020; Guo et al., 2020; Jean et al., 2020; Mehta et al., 2020; Yao et al., 2020), subsequent large-scale trials failed to demonstrate any benefit of the two antimalarials for SARS-CoV-2-infected patients (Borba et al., 2020; Hernandez et al., 2020; Horby et al., 2020; Pan et al., 2021). Similar disappointing results were obtained with hydroxychloroquine administered to macaque monkeys artificially infected with SARS-CoV-2 (Maisonnasse et al., 2020). SARS-CoV-2 infection association with endothelium damage (Wadman et al., 2020) and viral myocarditis (Chang et al., 2021; Topol, 2020), in combination with possible cardiomyopathy induced by chloroquine per se (Tönnesmann et al., 2013), represent further arguments against use of the two antimalarials in coronavirus-infected patients. The immunomodulatory effect of chloroquine via TLR7/TLR9 inhibition by impaired lysosomal acidification (In 't Veld et al., 2021; Kuznik et al., 2011; Tohmé and Manoury, 2014) may not be beneficial during coronavirus infection, since it was postulated that higher TLR7 expression in women vs. men via incomplete X chromosome inactivation may protect against viral infections including SARS-CoV-2 (Takahashi and Iwasaki, 2021).

5. Conclusions

In conclusion, we have shown via automated and manual patch-clamp experiments on cell lines expressing human cardiac ion channels and hiPSC-CM multiple inhibitory effects of chloroquine and hydroxychloroquine. We also produced direct estimates of hERG

blocking and unblocking rates via onset-of-block kinetics analysis. Proarrhythmogenic risk predictors B_{net} and Q_{net} computed based on these data provided similar results, placing the two compounds in the intermediate proarrhythmogenic risk group. In addition, we studied the voltage dependence of hERG block and also provided evidence for drug-induced hyperpolarizing shifts in voltage-dependent activation of hERG channels, as well as smaller hyperpolarizing shifts of voltage-dependent inactivation of hNav1.5 channels. However, these shifts applied to *in silico* simulations produced only small changes in Q_{net} values. Overall, we proved that CiPA-based methods can be combined and effectively used for proarrhythmogenic risk prediction in a real-life example.

CRediT authorship contribution statement

Urs Thomet: Conceptualization, Methodology, Investigation, Validation, Formal analysis, Data curation, Resources. **Bogdan Amuzescu:** Conceptualization, Methodology, Investigation, Validation, Formal analysis, Data curation, Software, Writing – original draft, Supervision. **Thomas Knott:** Conceptualization, Methodology, Validation, Formal analysis, Data curation, Resources, Writing – review & editing. **Stefan A. Mann:** Conceptualization, Methodology, Investigation, Validation, Formal analysis, Writing – review & editing. **Kanigula Mubagwa:** Conceptualization, Methodology, Validation, Formal analysis, Writing – review & editing, Supervision. **Beatrice Mihaela Radu:** Conceptualization, Methodology, Validation, Formal analysis, Writing – review & editing, Project administration, Funding acquisition.

Declaration of competing interest

The authors declare that they have no known competing financial interests or personal relationships that could have appeared to influence the work reported in this paper.

TK is CSO of CytoBioScience Inc. Part of the methods used within this study have been included in EPO patent application EP18465611.

Acknowledgements

Appendix A. Supplementary data

Supplementary data to this article can be found online at https://doi.org/10.1016/j.ejphar.2021.174632.

References

Airini, R., Iordache, F., Alexandru, D., Savu, L., Epureanu, F.B., Mihailescu, D., Amuzescu, B., Maniu, H., 2019. Senescence-induced immunophenotype, gene expression and electrophysiology changes in human amniocytes. J. Cell Mol. Med. 23, 7233–7245. https://doi.org/10.1111/jcmm.14495.

Amuzescu, B., Segal, A., Flonta, M.L., Simaels, J., Van Driessche, W., 2003. Zinc is a voltage-dependent blocker of native and heterologously expressed epithelial Na+ channels. Pflügers Archiv 446, 69–77. https://doi.org/10.1007/s00424-002-0998-3.

Amuzescu, B., Airini, R., Epureanu, F.B., Mann, S.A., Knott, T., Radu, B.M., 2021. Evolution of mathematical models of cardiomyocyte electrophysiology. Math. Biosci. 334, 108567. https://doi.org/10.1016/j.mbs.2021.108567.

Becker, M.L., Snijders, D., van Gemeren, C.W., Kingma, H.J., van Lelyveld, S.F.L., Giezen, T.J., 2021. QTc prolongation in COVID-19 patients using chloroquine. Cardiovasc. Toxicol. 2, 1–8. https://doi.org/10.1007/s12012-020-09621-2.

Borba, M.G.S., Val, F.F.A., Sampaio, V.S., Alexandre, M.A.A., Melo, G.C., Brito, M., Mourão, M.P.G., Brito-Sousa, J.D., Baía-da-Silva, D., Guerra, M.V.F., Hajjar, L.A., Pinto, R.C., Balieiro, A.A.S., Pacheco, A.G.F., Santos Jr., J.D.O., Naveca, F.G., Xavier, M.S., Siqueira, A.M., Schwarzbold, A., Croda, J., Nogueira, M.L., Romero, G.A.S., Bassat, Q., Fontes, C.J., Albuquerque, B.C., Daniel-Ribeiro, C.T., Monteiro, W.M., Lacerda, M.V.G., 2020. Effect of high vs low doses of chloroquine diphosphate as

adjunctive therapy for patients hospitalized with severe acute respiratory syndrome coronavirus 2 (SARS-CoV-2) infection: a randomized clinical trial. JAMA. Netw. Open. 3, 8857. https://doi.org/10.1001/jamanetworkopen.2020.8857.

Borsini, F., Crumb, W., Pace, S., Ubben, D., Wible, B., Yan, G.X., Funck-Brentano, C., 2012. In vitro cardiovascular effects of dihydroartemisin-piperaquine combination compared with other antimalarials. Antimicrob. Agents Chemother. 56, 3261–3270. https://doi.org/10.1128/AAC.05688-11.

Caballero, R., Gómez, R., Núñez, L., Moreno, I., Tamargo, J., Delpón, E., 2004. Diltiazem inhibits hKv1.5 and Kv4.3 currents at therapeutic concentrations. Cardiovasc. Res. 64, 457–466. https://doi.org/10.1016/j.cardiores.2004.07.022.

Capel, R.A., Herring, N., Kalla, M., Yavari, A., Mirams, G.R., Douglas, G., Bub, G., Channon, K., Paterson, D.J., Terrar, D.A., Burton, R.A., 2015. Hydroxychloroquine reduces heart rate by modulating the hyperpolarization-activated current If: novel electrophysiological insights and therapeutic potential. Heart Rhythm 12, 2186–2194. https://doi.org/10.1016/j.hrthm.2015.05.027.

Cardiac Arrhythmia Suppression Trial (CAST) Investigators, 1989. Preliminary report: effect of encainide and flecainide on mortality in a randomized trial of arrhythmia suppression after myocardial infarction. N. Engl. J. Med. 321, 406–412. https://doi.org/10.1056/NEJM198908103210629.

Carmeliet, E., 1992. Voltage- and time-dependent block of the delayed K+ current in cardiac myocytes by dofetilide. J. Pharmacol. Exp. Therapeut. 262, 809–817.

Carmeliet, E., 1993. Use-dependent block and use-dependent unblock of the delayed rectifier K+ current by almokalant in rabbit ventricular myocytes. Circ. Res. 73, 857–868. https://doi.org/10.1161/01.res.73.5.857.

Chang, W.T., Toh, H.S., Liao, C.T., Yu, W.L., 2021. Cardiac involvement of COVID-19: a comprehensive review. Am. J. Med. Sci. 361, 14–22. https://doi.org/10.1016/j.amjms.2020.10.002.

Chew, C.Y., Mar, A., Nikpour, M., Saracino, A.M., 2020. Hydroxychloroquine in dermatology: new perspectives on an old drug. Australas. J. Dermatol. 61, e150–e157. https://doi.org/10.1111/ajd.13168.

Chorin, E., Dai, M., Shulman, E., Wadhwani, L., Bar-Cohen, R., Barbhaiya, C., Aizer, A., Holmes, D., Bernstein, S., Spinelli, M., Park, D.S., Chinitz, L.A., Jankelson, L., 2020. The QT interval in patients with COVID-19 treated with hydroxychloroquine and azithromycin. Nat. Med. 26, 808–809. https://doi.org/10.1038/s41591-020-0888-2.

Cook, J.A., Randinitis, E.J., Bramson, C.R., Wesche, D.L., 2006. Lack of a pharmacokinetic interaction between azithromycin and chloroquine. Am. J. Trop. Med. Hyg. 74, 407–412.

Delaunois, A., Abernathy, M., Anderson, W.D., Beattie, K.A., Chaudhary, K.W., Coulot, J., Gryshkova, V., Hebeisen, S., Holbrook, M., Kramer, J., Kuryshev, Y., Leishman, D., Lushbough, I., Passini, E., Redfern, W.S., Rodriguez, B., Rossman, E.I., Trovato, C., Wu, C., Valentin, J.P., 2021. Applying the CiPA approach to evaluate cardiac proarrhythmia risk of some antimalarials used off-label in the first wave of COVID-19. Clin. Transl. Sci 2021. 13011. https://doi.org/10.1111/cts.13011.

Ducharme, J., Farinotti, R., 1996. Clinical pharmacokinetics and metabolism of chloroquine. Focus on recent advancements. Clin. Pharmacokinet. 31, 257–274. https://doi.org/10.2165/00003088-199631040-00003.

Dutta, S., Chang, K.C., Beattie, K.A., Sheng, J., Tran, P.N., Wu, W.W., Wu, M., Strauss, D.G., Colatsky, T., Li, Z., 2017. Optimization of an in silico cardiac cell model for proarrhythmia risk assessment. Front. Physiol. 8, 616. https://doi.org/10.3389/fphys.2017.00616.

Farias, K.J., Machado, P.R., Muniz, J.A., Imbeloni, A.A., da Fonseca, B.A., 2015. Antiviral activity of chloroquine against dengue virus type 2 replication in Aotus monkeys. Viral Immunol. 28, 161–169. https://doi.org/10.1089/vim.2014.0090.

Fermini, B., Hancox, J.C., Abi-Gerges, N., Bridgland-Taylor, M., Chaudhary, K.W., Colatsky, T., Correll, K., Crumb, W., Damiano, B., Erdemli, G., Gintant, G., Imredy, J., Koerner, J., Kramer, J., Levesque, P., Li, Z., Lindqvist, A., Obejero-Paz, C. A., Rampe, D., Sawada, K., Strauss, D.G., Vandenberg, J.I., 2016. A new perspective in the field of cardiac safety testing through the comprehensive in vitro proarrhythmia assay paradigm. J. Biomol. Screen 21, 1–11. https://doi.org/10.1177/1087057115594589.

Filgueiras-Rama, D., Martins, R.P., Mironov, S., Yamazaki, M., Calvo, C.J., Ennis, S.R., Bandaru, K., Noujaim, S.F., Kalifa, J., Berenfeld, O., Jalife, J., 2012. Chloroquine terminates stretch-induced atrial fibrillation more effectively than flecainide in the sheep heart. Circ. Arrhythm. Electrophysiol. 5, 561–570. https://doi.org/10.1161/CIRCEP.111.966820.

Gao, J., Tian, Z., Yang, X., 2020. Breakthrough: chloroquine phosphate has shown apparent efficacy in treatment of COVID-19 associated pneumonia in clinical studies. Biosci. Trends. 14, 72–73. https://doi.org/10.5582/bst.2020.01047.

Gasmi, A., Peana, M., Noor, S., Lysiuk, R., Menzel, A., Gasmi Benahmed, A., Bjørklund, G., 2021. Chloroquine and hydroxychloroquine in the treatment of COVID-19: the never-ending story. Appl. Microbiol. Biotechnol. 30, 1–11. https://doi.org/10.1007/s00253-021-11094-4.

Gérard, A., Romani, S., Fresse, A., Viard, D., Parassol, N., Granvuillemin, A., Chouchana, L., Rocher, F., Drici, M.D., 2020. Off-label" use of hydroxychloroquine, azithromycin, lopinavir-ritonavir and chloroquine in COVID-19: a survey of cardiac adverse drug reactions by the French Network of Pharmacovigilance Centers. Therapie 75, 371–379. https://doi.org/10.1016/j.therap.2020.05.002.

Gessner, G., Macianskiene, R., Starkus, J.G., Schönherr, R., Heinemann, S.H., 2010. The amiodarone derivative KB130015 activates hERG1 potassium channels via a novel mechanism. Eur. J. Pharmacol. 632, 52–59. https://doi.org/10.1016/j.ejphar.2010.01.010.

Gomis-Tena, J., Brown, B.M., Cano, J., Trenor, B., Yang, P.C., Saiz, J., Clancy, C.E., Romero, L., 2020. When does the IC(50) accurately assess the blocking potency of a drug? J. Chem. Inf. Model. 60, 1779–1790. https://doi.org/10.1021/acs.jcim.9b01085.

Grandvuillemin, A., Drici, M.D., Jonville-Bera, A.P., Micallef, J., Montastruc, J.L., 2021. French pharmacovigilance public system and COVID-19 pandemic. Drug Saf. 44, 405–408. https://doi.org/10.1007/s40264-020-01034-y.

Guo, Y.R., Cao, Q.D., Hong, Z.S., Tan, Y.Y., Chen, S.D., Jin, H.J., Tan, K.S., Wang, D.Y., Yan, Y., 2020. The origin, transmission and clinical therapies on coronavirus disease 2019 (COVID-19) outbreak - an update on the status. Mil Med Res 7, 11. https://doi.org/10.1186/s40779-020-00240-0.

Haładyj, E., Sikora, M., Felis-Giemza, A., Olesińska, M., 2018. Antimalarials - are they effective and safe in rheumatic diseases? Reumatologia 56, 164–173. https://doi.org/10.5114/reum.2018.76904.

Han, X., Samieegohar, M., Ridder, B.J., Wu, W.W., Randolph, A., Tran, P., Sheng, J., Stoelzle-Feix, S., Brinkwirth, N., Rotordam, M.G., Becker, N., Friis, S., Rapedius, M., Goetze, T.A., Strassmaier, T., Okeyo, G., Kramer, J., Kuryshev, Y., Wu, C., Strauss, D. G., Li, Z., 2020. A general procedure to select calibration drugs for lab-specific validation and calibration of proarrhythmia risk prediction models: an illustrative example using the CiPA model. J. Pharmacol. Toxicol. Methods 105, 106890. https://doi.org/10.1016/j.vascn.2020.106890.

Hernandez, A.V., Roman, Y.M., Pasupuleti, V., Barboza, J.J., White, C.M., 2020. Update alert 3: hydroxychloroquine or chloroquine for the treatment or prophylaxis of COVID-19. Ann. Intern. Med. 173, W156–W157. https://doi.org/10.7326/L20-1257.

Horby, P., Mafham, M., Linsell, L., Bell, J.L., Staplin, N., Emberson, J.R., Wiselka, M., Ustianowski, A., Elmahi, E., Prudon, B., Whitehouse, T., Felton, T., Williams, J., Faccenda, J., Underwood, J., Baillie, J.K., Chappell, L.C., Faust, S.N., Jaki, T., Jeffery, K., Lim, W.S., Montgomery, A., Rowan, K., Tarning, J., Watson, J.A., White, N.J., Juszczak, E., Haynes, R., Landray, M.J., 2020. Effect of hydroxychloroquine in hospitalized patients with covid-19. N. Engl. J. Med. 383, 2030–2040. https://doi.org/10.1056/NEJMoa2022926.

Hosaka, Y., Iwata, M., Kamiya, N., Yamada, M., Kinoshita, K., Fukunishi, Y., Tsujimae, K., Hibino, H., Aizawa, Y., Inanobe, A., Nakamura, H., Kurachi, Y., 2007. Mutational analysis of block and facilitation of HERG current by a class III anti-arrhythmic agent. nifekalant. Channels (Austin) 1, 198–208. https://doi.org/10.4161/chan.4691.

In 't Veld, A.E., Jansen, M.A.A., Ciere, L.C.A., Moerland, M., 2021. Hydroxychloroquine effects on TLR signalling: underexposed but unneglectable in COVID-19. J Immunol Res 2021 6659410. https://doi.org/10.1155/2021/6659410.

Iordache, F., Constantinescu, A., Andrei, E., Amuzescu, B., Halitzchi, F., Savu, L., Maniu, H., 2016. Electrophysiology, immunophenotype, and gene expression characterization of senescent and cryopreserved human amniotic fluid stem cells. J. Physiol. Sci. 66, 463–476. https://doi.org/10.1007/s12576-016-0441-8.

Jean, S.S., Lee, P.I., Hsueh, P.R., 2020. Treatment options for COVID-19: the reality and challenges. J. Microbiol. Immunol. Infect. 53, 436–443. https://doi.org/10.1016/j.jmii.2020.03.034.

Jordaan, P., Dumotier, B., Traebert, M., Miller, P.E., Ghetti, A., Urban, L., Abi-Gerges, N., 2021. Cardiotoxic potential of hydroxychloroquine, chloroquine and azithromycin in adult human primary cardiomyocytes. Toxicol. Sci. https://doi.org/10.1093/toxsci/kfaa194, 2021.

Kashour, Z., Riaz, M., Garbati, M.A., AlDosary, O., Tlayjeh, H., Gerberi, D., Murad, M.H., Sohail, M.R., Kashour, T., Tleyjeh, I.M., 2021. Efficacy of chloroquine or hydroxychloroquine in COVID-19 patients: a systematic review and meta-analysis. J. Antimicrob. Chemother. 76, 30–42. https://doi.org/10.1093/jac/dkaa403.

Keyaerts, E., Vijgen, L., Maes, P., Neyts, J., Van Ranst, M., 2004. In vitro inhibition of severe acute respiratory syndrome coronavirus by chloroquine. Biochem. Biophys. Res. Commun. 323, 264–268. https://doi.org/10.1016/j.bbrc.2004.08.085.

Keyaerts, E., Li, S., Vijgen, L., Rysman, E., Verbeeck, J., Van Ranst, M., Maes, P., 2009. Antiviral activity of chloroquine against human coronavirus OC43 infection in newborn mice. Antimicrob. Agents Chemother. 53, 3416–3421. https://doi.org/10.1128/AAC.01509-08.

Krafts, K., Hempelmann, E., Skórska-Stania, A., 2012. From methylene blue to chloroquine: a brief review of the development of an antimalarial therapy. Parasitol. Res. 111, 1–6. https://doi.org/10.1007/s00436-012-2886-x.

Kuznik, A., Bencina, M., Svajger, U., Jeras, M., Rozman, B., Jerala, R., 2011. Mechanism of endosomal TLR inhibition by antimalarial drugs and imidazoquinolines. J. Immunol. 186, 4794–4804. https://doi.org/10.4049/jimmunol.1000702.

Lentini, G., Cavalluzzi, M.M., Habtemariam, S., 2020. COVID-19, chloroquine repurposing, and cardiac safety concern: chirality might help. Molecules 25. https://doi.org/10.3390/molecules25081834.

Li, C., Zhu, X., Ji, X., Quanquin, N., Deng, Y.Q., Tian, M., Aliyari, R., Zuo, X., Yuan, L., Afridi, S.K., Li, X.F., Jung, J.U., Nielsen-Saines, K., Qin, F.X., Qin, C.F., Xu, Z., Cheng, G., 2017a. Chloroquine, a FDA-approved drug, prevents Zika virus infection and its associated congenital microcephaly in mice. EBioMedicine 24, 189–194. https://doi.org/10.1016/j.ebiom.2017.09.034.

Li, Z., Dutta, S., Sheng, J., Tran, P.N., Wu, W., Chang, K., Mdluli, T., Strauss, D.G., Colatsky, T., 2017b. Improving the in silico assessment of proarrhythmia risk by combining hERG (human ether-a-go-go-related gene) channel-drug binding kinetics and multichannel pharmacology. Circ. Arrhythm. Electrophysiol. 10, e004628 https://doi.org/10.1161/CIRCEP.116.004628.

Li, Z., Mirams, G.R., Yoshinaga, T., Ridder, B.J., Han, X., Chen, J.E., Stockbridge, N.L., Wisialowski, T.A., Damiano, B., Severi, S., Morissette, P., Kowey, P.R., Holbrook, M., Smith, G., Rasmusson, R.L., Liu, M., Song, Z., Qu, Z., Leishman, D.J., Steidl-Nichols, J., Rodriguez, B., Bueno-Orovio, A., Zhou, X., Passini, E., Edwards, A.G., Morotti, S., Ni, H., Grandi, E., Clancy, C.E., Vandenberg, J., Hill, A., Nakamura, M., Singer, T., Polonchuk, L., Greiter-Wilke, A., Wang, K., Nave, S., Fullerton, A., Sobie, E.A., Paci, M., Musuamba Tshinanu, F., Strauss, D.G., 2020. General principles for the validation of proarrhythmia risk prediction models: an extension of the CiPA

in silico strategy. Clin. Pharmacol. Ther. 107, 102–111. https://doi.org/10.1002/cpt.1647.

Maisonnasse, P., Guedj, J., Contreras, V., Behillil, S., Solas, C., Marlin, R., Naninck, T., Pizzorno, A., Lemaitre, J., Gonçalves, A., Kahlaoui, N., Terrier, O., Fang, R.H.T., Enouf, V., Dereuddre-Bosquet, N., Brisebarre, A., Touret, F., Chapon, C., Hoen, B., Lina, B., Calatrava, M.R., van der Werf, S., de Lamballerie, X., Le Grand, R., 2020. Hydroxychloroquine use against SARS-CoV-2 infection in non-human primates. Nature 585, 584–587. https://doi.org/10.1038/s41586-020-2558-4.

Mann, S.A., Heide, J., Knott, T., Airini, R., Epureanu, F.B., Deftu, A.-F., Deftu, A.-T., Radu, B.M., Amuzescu, B., 2019. Recording of multiple ion current components and action potentials in human induced pluripotent stem cell-derived cardiomyocytes via automated patch-clamp. J. Pharmacol. Toxicol. Methods 100, 106599. https://doi.org/10.1016/j.vascn.2019.106599.

Mehra, M.R., Desai, S.S., Ruschitzka, F., Patel, A.N., 2020. RETRACTED: hydroxychloroquine or chloroquine with or without a macrolide for treatment of COVID-19: a multinational registry analysis. Lancet 6736, 31180–31186. https://doi.org/10.1016/S0140-6736(20)31180-6.

Mehta, N., Mazer-Amirshahi, M., Alkindi, N., Pourmand, A., 2020. Pharmacotherapy in COVID-19; A narrative review for emergency providers. Am. J. Emerg. Med. 38, 1488–1493. https://doi.org/10.1016/j.ajem.2020.04.035.

Mercuro, N.J., Yen, C.F., Shim, D.J., Maher, T.R., McCoy, C.M., Zimetbaum, P.J., Gold, H.S., 2020. Risk of QT interval prolongation associated with use of hydroxychloroquine with or without concomitant azithromycin among hospitalized patients testing positive for coronavirus disease 2019 (COVID-19). JAMA Cardiol 5, 1036–1041. https://doi.org/10.1001/jamacardio.2020.1834.

Milnes, J.T., Witchel, H.J., Leaney, J.L., Leishman, D.J., Hancox, J.C., 2010. Investigating dynamic protocol-dependence of hERG potassium channel inhibition at 37 degrees C: cisapride versus dofetilide. J. Pharmacol. Toxicol. Methods 61, 178–191. https://doi.org/10.1016/j.vascn.2010.02.007.

Mistry, H.B., 2018. Complex versus simple models: ion-channel cardiac toxicity prediction. PeerJ 6, e4352. https://doi.org/10.7717/peerj.4352.

Mistry, H.B., 2019. Comprehensive in vitro proarrhythmic assay complexity bias. Clin. Pharmacol. Ther. 105, 1323–1324. https://doi.org/10.1002/cpt.1400.

Mitcheson, J.S., Chen, J., Sanguinetti, M.C., 2000. Trapping of a methanesulfonanilide by closure of the HERG potassium channel activation gate. J. Gen. Physiol. 115, 229–240. https://doi.org/10.1085/jgp.115.3.229.

Montnach, J., Baró, I., Charpentier, F., De Waard, M., Loussouarn, G., 2021. Modelling sudden cardiac death risks factors in patients with coronavirus disease of 2019: the hydroxychloroquine and azithromycin case. Europace 2021 euab043. https://doi.org/10.1093/europace/euab043.

Mubagwa, K., 2020. Cardiac effects and toxicity of chloroquine: a short update. Int. J. Antimicrob. Agents 56, 19. https://doi.org/10.1016/j.ijantimicag.2020.106057.

Noujaim, S.F., Stuckey, J.A., Ponce-Balbuena, D., Ferrer-Villada, T., López-Izquierdo, A., Pandit, S.V., Sánchez-Chapula, J.A., Jalife, J., 2011. Structural bases for the different anti-fibrillatory effects of chloroquine and quinidine. Cardiovasc. Res. 89, 862–869. https://doi.org/10.1093/cvr/cvr008.

O'Hara, T., Virág, L., Varró, A., Rudy, Y., 2011. Simulation of the undiseased human cardiac ventricular action potential: model formulation and experimental validation. PLoS Comput. Biol. 7, e1002061 https://doi.org/10.1371/journal.pcbi.1002061.

Pan, H., Peto, R., Henao-Restrepo, A.M., Preziosi, M.P., Sathiyamoorthy, V., Abdool Karim, Q., Alejandria, M.M., Hernández García, C., Kieny, M.P., Malekzadeh, R., Murthy, S., Reddy, K.S., Roses Periago, M., Abi Hanna, P., Ader, F., Al-Bader, A.M., Alhasawi, A., Allum, E., Alotaibi, A., Alvarez-Moreno, C.A., Appadoo, S., Asiri, A., Aukrust, P., Barratt-Due, A., Bellani, S., Branca, M., Cappel-Porter, H.B.C., Cerrato, N., Chow, T.S., Como, N., Eustace, J., García, P.J., Godbole, S., Gotuzzo, E., Griskevicius, L., Hamra, R., Hassan, M., Hassany, M., Hutton, D., Irmansyah, I., Jancoriene, L., Kirwan, J., Kumar, S., Lennon, P., Lopardo, G., Lydon, P., Magrini, N., Maguire, T., Manevska, S., Manuel, O., McGinty, S., Medina, M.T., Mesa Rubio, M.L., Miranda-Montoya, M.C., Nel, J., Nunes, E.P., Perola, M., Portolés, A., Rasmin, M.R., Raza, A., Rees, H., Reges, P.P.S., Rogers, C.A., Salami, K., Salvadori, M.I., Sinani, N., Sterne, J.A.C., Stevanovikj, M., Tacconelli, E., Tikkinen, K.A.O., Trelle, S., Zaid, H., Røttingen, J.-A., Swaminathan, S., 2021. Repurposed antiviral drugs for covid-19 - interim WHO solidarity trial results. N. Engl. J. Med. 384, 497–511. https://doi.org/10.1056/NEJMoa2023184.

Parikh, J., Di Achille, P., Kozloski, J., Gurev, V., 2019. Global sensitivity analysis of ventricular myocyte model-derived metrics for proarrhythmic risk assessment. Front. Pharmacol. 10, 1054. https://doi.org/10.3389/fphar.2019.01054.

Perrin, M.J., Kuchel, P.W., Campbell, T.J., Vandenberg, J.I., 2008. Drug binding to the inactivated state is necessary but not sufficient for high-affinity binding to human ether-À -go-go-related gene channels. Mol. Pharmacol. 74, 1443–1452. https://doi.org/10.1124/mol.108.049056.

Perry, M., Sachse, F.B., Abbruzzese, J., Sanguinetti, M.C., 2009. PD-118057 contacts the pore helix of hERG1 channels to attenuate inactivation and enhance K+ conductance. Proc. Natl. Acad. Sci. U. S. A. 106, 20075–20080. https://doi.org/10.1073/pnas.0906597106.

Perry, M., Sanguinetti, M., Mitcheson, J., 2010. Revealing the structural basis of action of hERG potassium channel activators and blockers. J. Physiol. 588, 3157–3167. https://doi.org/10.1113/jphysiol.2010.194670.

Piller, C., 2021. Disgraced COVID-19 studies are still routinely cited. Science 371, 331–332. https://doi.org/10.1126/science.371.6527.331.

Pritchett, D.B., Sontheimer, H., Gorman, C.M., Kettenmann, H., Seeburg, P.H., Schofield, P.R., 1988. Transient expression shows ligand gating and allosteric potentiation of GABAA receptor subunits. Science 242, 1306–1308. https://doi.org/10.1126/science.2848320.

Reid, G., Amuzescu, B., Zech, E., Flonta, M.L., 2001. A system for applying rapid warming or cooling stimuli to cells during patch clamp recording or ion imaging. J. Neurosci. Methods 111, 1–8. https://doi.org/10.1016/s0165-0270(01)00416-2.

Roden, D.M., Harrington, R.A., Poppas, A., Russo, A.M., 2020. Considerations for drug interactions on QTc interval in exploratory COVID-19 treatment. J. Am. Coll. Cardiol. 75, 2623–2624. https://doi.org/10.1016/j.jacc.2020.04.016.

Rodríguez-Menchaca, A.A., Navarro-Polanco, R.A., Ferrer-Villada, T., Rupp, J., Sachse, F. B., Tristani-Firouzi, M., Sánchez-Chapula, J.A., 2008. The molecular basis of chloroquine block of the inward rectifier Kir2.1 channel. Proc. Natl. Acad. Sci. U. S. A. 105, 1364–1368. https://doi.org/10.1073/pnas.0708153105.

Sager, P.T., Gintant, G., Turner, J.R., Pettit, S., Stockbridge, N., 2014. Rechanneling the cardiac proarrhythmia safety paradigm: a meeting report from the Cardiac Safety Research Consortium. Am. Heart J. 167, 292–300.

Sánchez-Chapula, J.A., Salinas-Stefanon, E., Torres-Jácome, J., Benavides-Haro, D.E., Navarro-Polanco, R.A., 2001. Blockade of currents by the antimalarial drug chloroquine in feline ventricular myocytes. J. Pharmacol. Exp. Therapeut. 297, 437–445.

Sánchez-Chapula, J.A., Navarro-Polanco, R.A., Culberson, C., Chen, J., Sanguinetti, M.C., 2002. Molecular determinants of voltage-dependent human ether-a-go-go related gene (HERG) K+ channel block. J. Biol. Chem. 277, 23587–23595. https://doi.org/10.1074/jbc.M200448200.

Sánchez-Chapula, J.A., Navarro-Polanco, R.A., Sanguinetti, M.C., 2004. Block of wild-type and inactivation-deficient human ether-a-go-go-related gene K+ channels by halofantrine. Naunyn-Schmiedeberg's Arch. Pharmacol. 370, 484–491. https://doi.org/10.1007/s00210-004-0995-5.

Scheel, O., Frech, S., Amuzescu, B., Eisfeld, J., Lin, K.H., Knott, T., 2014. Action potential characterization of human induced pluripotent stem cell-derived cardiomyocytes using automated patch-clamp technology. Assay Drug Dev. Technol. 12, 457–469. https://doi.org/10.1089/adt.2014.601.

Stett, A., Burkhardt, C., Weber, U., van Stiphout, P., Knott, T., 2003. CYTOCENTERING: a novel technique enabling automated cell-by-cell patch clamping with the CYTOPATCH chip. Recept. Channel 9, 59–66. https://doi.org/10.3109/10606820308254.

Takahashi, T., Iwasaki, A., 2021. Sex differences in immune responses. Science 371, 347–348. https://doi.org/10.1126/science.abe7199.

TeBay, C., McArthur, J., Mangala, M., Kerr, N., Heitmann, S., Perry, M., Windley, M.J., Vandenberg, J.I., Hill, A.P., 2021. Comprehensive preclinical evaluation of how cardiac safety profiles of potential COVID-19 drugs are modified by disease associated factors. Authorea February 25. https://doi.org/10.22541/au.161429217.72966648/v1.

Tleyjeh, I.M., Kashour, Z., AlDosary, O., Riaz, M., Tlayjeh, H., Garbati, M.A., Tleyjeh, R., Al-Mallah, M.H., Sohail, M.R., Gerberi, D., Bin Abdulhak, A.A., Giudicessi, J.R., Ackerman, M.J., Kashour, T., 2020. The cardiac toxicity of chloroquine or hydroxychloroquine in COVID-19 patients: a systematic review and meta-regression analysis. Mayo Clin Proc Innov Qual Outcomes. https://doi.org/10.1016/j.mayocpiqo.2020.10.005 online ahead of print, 2020.

Tohmé, M., Manoury, B., 2014. Intracellular Toll-like receptor recruitment and cleavage in endosomal/lysosomal organelles. Methods Enzymol. 535, 141–147. https://doi.org/10.1016/B978-0-12-397925-4.00009-2.

Tönnesmann, E., Kandolf, R., Lewalter, T., 2013. Chloroquine cardiomyopathy - a review of the literature. Immunopharmacol. Immunotoxicol. 35, 434–442. https://doi.org/10.3109/08923973.2013.780078.

Topol, E.J., 2020. COVID-19 can affect the heart. Science 370, 408–409. https://doi.org/10.1126/science.abe2813.

Traebert, M., Dumotier, B., Meister, L., Hoffmann, P., Dominguez-Estevez, M., Suter, W., 2004. Inhibition of hERG K+ currents by antimalarial drugs in stably transfected HEK293 cells. Eur. J. Pharmacol. 484, 41–48. https://doi.org/10.1016/j.ejphar.2003.11.003.

US Food and Drug Administration, 2020. Fact sheet for health care providers emergency use authorization (EUA) of hydroxychloroquine sulfate supplied from the strategic national stockpile for treatment of COVID-19 in certain hospitalised patients. June 15. https://www.fda.gov/media/136537/download.

Vandenberg, J.I., Perry, M.D., Perrin, M.J., Mann, S.A., Ke, Y., Hill, A.P., 2012. hERG K(+) channels: structure, function, and clinical significance. Physiol. Rev. 92, 1393–1478. https://doi.org/10.1152/physrev.00036.2011.

Varshneya, M., Irurzun-Arana, I., Campana, C., Dariolli, R., Gutierrez, A., Pullinger, T.K., Sobie, E.A., 2021. Investigational treatments for COVID-19 may increase ventricular arrhythmia risk through drug interactions. CPT Pharmacometrics Syst. Pharmacol. 10, 100–107. https://doi.org/10.1002/psp4.12573.

Verdoorn, T.A., Draguhn, A., Ymer, S., Seeburg, P.H., Sakmann, B., 1990. Functional properties of recombinant rat GABAA receptors depend upon subunit composition. Neuron 4, 919–928. https://doi.org/10.1016/0896-6273(90)90145-6.

Vicente, J., Zusterzeel, R., Johannesen, L., Ochoa-Jimenez, R., Mason, J.W., Sanabria, C., Kemp, S., Sager, P.T., Patel, V., Matta, M.K., Liu, J., Florian, J., Garnett, C., Stockbridge, N., Strauss, D.G., 2019. Assessment of multi-ion channel block in a phase I randomized study design: results of the CiPA phase I ECG biomarker validation study. Clin. Pharmacol. Ther. 105, 943–953. https://doi.org/10.1002/cpt.1303.

Vincent, M.J., Bergeron, E., Benjannet, S., Erickson, B.R., Rollin, P.E., Ksiazek, T.G., Seidah, N.G., Nichol, S.T., 2005. Chloroquine is a potent inhibitor of SARS coronavirus infection and spread. Virol. J. 2, 69. https://doi.org/10.1186/1743-422X-2-69.

Wadman, M., Couzin-Frankel, J., Kaiser, J., Matacic, C., 2020. A rampage through the body. Science 368, 356–360. https://doi.org/10.1126/science.368.6489.356.

Wagner, M., Riepe, K.G., Eberhardt, E., Volk, T., 2010. Open channel block of the fast transient outward K+ current by primaquine and chloroquine in rat left ventricular cardiomyocytes. Eur. J. Pharmacol. 647, 13–20. https://doi.org/10.1016/j.ejphar.2010.08.007.

Wallace, D.J., 1989. The use of quinacrine (Atabrine) in rheumatic diseases: a reexamination. Semin. Arthritis Rheum. 18, 282–296. https://doi.org/10.1016/0049-0172(89)90050-4.

Wang, M., Cao, R., Zhang, L., Yang, X., Liu, J., Xu, M., Shi, Z., Hu, Z., Zhong, W., Xiao, G., 2020. Remdesivir and chloroquine effectively inhibit the recently emerged novel coronavirus (2019-nCoV) in vitro. Cell Res. 30, 269–271. https://doi.org/10.1038/s41422-020-0282-0.

Whittaker, D.G., Capel, R.A., Hendrix, M., Chan, X.H.S., Herring, N., White, N.J., Mirams, G.R., Burton, R.B., 2021. Cardiac TdP risk stratification modelling of anti-infective compounds including chloroquine and hydroxychloroquine. R Soc Open Sci 8, 210235.

Williams, G., Mirams, G.R., 2015. A web portal for in-silico action potential predictions. J. Pharmacol. Toxicol. Methods 75, 10–16. https://doi.org/10.1016/j.vascn.2015.05.002.

Windley, M.J., Abi-Gerges, N., Fermini, B., Hancox, J.C., Vandenberg, J.I., Hill, A.P., 2017. Measuring kinetics and potency of hERG block for CiPA. J. Pharmacol. Toxicol. Methods 87, 99–107. https://doi.org/10.1016/j.vascn.2017.02.017.

Windley, M.J., Lee, W., Vandenberg, J.I., Hill, A.P., 2018. The temperature dependence of kinetics associated with drug block of hERG channels is compound-specific and an important factor for proarrhythmic risk prediction. Mol. Pharmacol. 94, 760–769. https://doi.org/10.1124/mol.117.111534.

Woodhull, A.M., 1973. Ionic blockage of sodium channels in nerve. J. Gen. Physiol. 61, 687–708. https://doi.org/10.1085/jgp.61.6.687.

Yan, Y., Zou, Z., Sun, Y., Li, X., Xu, K.F., Wei, Y., Jin, N., Jiang, C., 2013. Anti-malaria drug chloroquine is highly effective in treating avian influenza A H5N1 virus infection in an animal model. Cell Res. 23, 300–302. https://doi.org/10.1038/cr.2012.165.

Yao, X., Ye, F., Zhang, M., Cui, C., Huang, B., Niu, P., Liu, X., Zhao, L., Dong, E., Song, C., Zhan, S., Lu, R., Li, H., Tan, W., Liu, D., 2020. In vitro antiviral activity and projection of optimized dosing design of hydroxychloroquine for the treatment of severe acute respiratory syndrome coronavirus 2 (SARS-CoV-2). Clin. Infect. Dis. 71, 732–739. https://doi.org/10.1093/cid/ciaa237.

Yuan, S., Chan, J.F.W., Chik, K.K.H., Chan, C.C.Y., Tsang, J.O.L., Liang, R., Cao, J., Tang, K., Chen, L.L., Wen, K., Cai, J.P., Ye, Z.W., Lu, G., Chu, H., Jin, D.Y., Yuen, K. Y., 2020. Discovery of the FDA-approved drugs bexarotene, cetilistat, diiodohydroxyquinoline, and abiraterone as potential COVID-19 treatments with a robust two-tier screening system. Pharmacol. Res. 159, 104960. https://doi.org/10.1016/j.phrs.2020.104960.